Journal of Biomolecular Structure and Dynamics

ISSN: 0739-1102 (Print) 1538-0254 (Online) Journal homepage: www.tandfonline.com/journals/tbsd20

Structural insights into modeling of hepatitis B virus reverse transcriptase and identification of its inhibitors from potential medicinal plants of Western Ghats: an *in silico* and *in vitro* study

Vishal S. Patil, Darasaguppe R. Harish, Rajitha Charla, Umashankar Vetrivel, Sunil S. Jalalpure, Vishwambhar Vishnu Bhandare, Sanjay H. Deshpande, Harsha V. Hegde & Subarna Roy

To cite this article: Vishal S. Patil, Darasaguppe R. Harish, Rajitha Charla, Umashankar Vetrivel, Sunil S. Jalalpure, Vishwambhar Vishnu Bhandare, Sanjay H. Deshpande, Harsha V. Hegde & Subarna Roy (2024) Structural insights into modeling of hepatitis B virus reverse transcriptase and identification of its inhibitors from potential medicinal plants of Western Ghats: an *in silico* and *in vitro* study, Journal of Biomolecular Structure and Dynamics, 42:21, 11731-11749, DOI: 10.1080/07391102.2023.2264400

To link to this article: https://doi.org/10.1080/07391102.2023.2264400

JOURNAL OF BIOMOLECULAR STRUCTURE AND DYNAMICS
2024, VOL. 42, NO. 21, 11731–11749
https://doi.org/10.1080/07391102.2023.2264400

Structural insights into modeling of hepatitis B virus reverse transcriptase and identification of its inhibitors from potential medicinal plants of Western Ghats: an *in silico* and *in vitro* study

Vishal S. Patil[a,b], Darasaguppe R. Harish[a], Rajitha Charla[a], Umashankar Vetrivel[a,c], Sunil S. Jalalpure[b], Vishwambhar Vishnu Bhandare[a,d], Sanjay H. Deshpande[a,e], Harsha V. Hegde[a] and Subarna Roy[a]

[a]ICMR-National Institute of Traditional Medicine, Belagavi, Karnataka, India; [b]KLE College of Pharmacy, Belagavi, KLE Academy of Higher Education and Research, Belagavi, Karnataka, India; [c]ICMR-National Institute for Research in Tuberculosis, Chennai, Tamil Nadu, India; [d]Department of Microbiology, Shivaji University, Kolhapur, Maharashtra, India; [e]Regional Centre for Biotechnology, NCR-Biotech Science Cluster, Faridabad, India

Communicated by Ramaswamy H. Sarma

ABSTRACT

The present study was proposed to model full-length HBV-RT and investigate the intermolecular interactions of known inhibitor and libraries of phytocompounds to probe the potential natural leads by *in silico* and *in vitro* studies. Homology modeling of RT was performed by Phyre2 and Modeller and virtual screening of ligands implemented through POAP pipeline. Molecular dynamics (MD) simulation (100 ns) and MM-GBSA calculations were performed using Schrodinger Desmond and Prime, respectively. Phytocompounds probable host protein targets gene set pathway enrichment and network analysis were executed by KEGG database and Cytoscape software. Prioritized plant extracts/enriched fraction LC-MS analysis was performed and along with pure compound, RT inhibitory activity, time-dependent HBsAg and HBeAg secretion, and intracellular HBV DNA, and pgRNA by qRT-PCR was performed in HepG2.2.15 cell line. Among the screened chemical library of 268 phytocompounds from 18 medicinal plants, 15 molecules from *Terminalia chebula* (6), *Bidens pilosa* (5), and *Centella asiatica* (4)) were identified as potential inhibitors of YMDD and RT1 motif of HBV-RT. MD simulation demonstrated stable interactions of 15 phytocompounds with HBV-RT, of which 1,2,3,4,6-Pentagalloyl Glucose (PGG) was identified as lead molecule. Out of 15 compounds, 11 were predicted to modulate 39 proteins and 15 molecular pathways associated with HBV infection. TCN and TCW (500 µg/mL) showed potent RT inhibition, decreased intracellular HBV DNA, and pgRNA, and time-dependent inhibition of HBsAg and HBeAg levels compared to PGG and Tenofovir Disoproxil Fumarate. We propose that the identified lead molecules from *T. chebula* as promising and cost-effective moieties for the management of HBV infection.

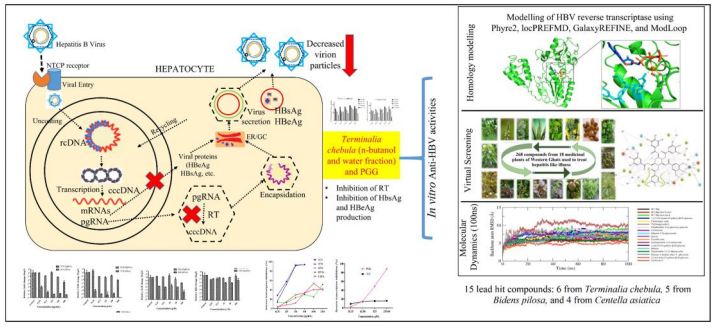

Abbreviations: BPHA: *B. pilosa* hydroalcoholic; BPM: *B. pilosa* methanolic; CAHA: *C. asiatica* hydroalcoholic; cccDNA: covalently closed circular DNA; DNA Pol: DNA polymerase; HBeAg: hepatitis B e-antigen; HBsAg: hepatitis B surface antigen; HBV: hepatitis B virus; KEGG: Kyoto Encyclopedia of Genes and Genomes; LC-MS: liquid chromatography-mass spectrometry; locPREFMD: local protein structure refinement *via* molecular dynamics; MD: molecular dynamics; MM-GBSA: molecular mechanics with generalised born and surface area solvation; NTCP: sodium taurocholate co-transporting polypeptide; PCIDB: phytochemical interactions DB; PE: potential energy; PGG: pentagalloylglucose; pgRNA: pregenomic

ARTICLE HISTORY
Received 7 July 2023
Accepted 21 September 2023

KEYWORDS
Hepatitis B; HepG2.2.15 cell line; molecular modeling; reverse transcriptase; *Terminalia chebula*

CONTACT Darasaguppe R. Harish harish.dr@icmr.gov.in ICMR-National Institute of Traditional Medicine, Nehru Nagar, Belagavi, Karnataka, 590010, India; Sunil S. Jalalpure jalalpuresunil@rediffmail.com KLE College of Pharmacy, Belagavi, KLE Academy of Higher Education and Research, Nehru Nagar, Belagavi, Karnataka, 590010, India.

Supplemental data for this article can be accessed online at https://doi.org/10.1080/07391102.2023.2264400.

RNA; rcDNA: relaxed circular DNA; RMSD: root-mean-square-deviation; RMSF: root-mean-square-fluctuation; RT: reverse transcriptase; TCN: *T. chebula* n-butanol fraction; TCW: *T. chebula* water fraction; TDF: tenofovir disoproxil fumarate; YMDD: tyrosine (Y)-methionine (M)-aspartic acid (D)-aspartic acid (D).

1. Introduction

Viral hepatitis is an inflammation of the liver caused by five major hepatitis viruses, namely hepatitis A, B, C, D, and E. These viruses primarily infect and replicate within the hepatocytes of the liver. All these five viruses are from different viral families and have diverse molecular properties, but similar clinical symptoms (Louten, 2016; Tu et al., 2017). Among these, the hepatitis B virus (HBV) is considered a major public health threat and causes variable degrees of liver diseases (acute to chronic hepatitis), liver fibrosis, cirrhosis, and hepatocellular carcinoma (HCC) (Coffin et al., 2021; Nelson et al., 2016). HBV has an affinity for hepatocytes, studies also infer that small amounts of HBV DNA to be found in the pancreas, mononuclear cells, and kidney (Stein & Loomba, 2009). According to an estimate made by the World Health Organisation (WHO), >2 billion people were currently infected, and about 360 million were living with chronic HBV infection (World Health Organization, 2021), thereby becomes the tenth highest number of deaths worldwide with ~7,80,000 HBV-related global deaths being documented every year. In developed countries, young adults are more at risk due to higher sexual activities and injectable drug abuse. However, in East Asian countries and sub-Saharan Africa transmission through perinatal or horizontal routes are common (Jefferies et al., 2018; Zhang et al., 2018).

The US Food and Drug Administration (FDA) has approved several anti-viral drugs for the treatment of HBV infection. Broadly, interferons and nucleoside/nucleotide analogs (NAs), such as lamivudine, entecavir, adefovir dipivoxil, telbivudine, tenofovir disoproxil fumatate, and tenofovir alafenamide (Hepatitis B Foundation, 2022). NAs inhibit the reverse transcriptase of the HBV polymerase. However, the use of these agents is limited due to the requirement of high-dose to inhibit the viral reactivation, development of drug resistance due to the mutation in the polymerase gene, difficulties in dealing with high viral load, and increased serum ALT leading to the progression of liver disease (Fontana, 2009; Zoulim & Locarnini, 2009). NAs are also associated with numerous adverse reactions in patients with long therapy and have a Black Box warning due to their potential antagonist effect on human DNA Pol-γ which is involved in mitochondrial DNA replication, leading to the reduced level of intracellular mitochondrial DNA. Furthermore, it causes mitochondrial toxicity, i.e. neuropathy, myopathy, and lactic acidosis. HBV therapy requires the elimination of the covalently closed circular (cccDNA) from infected cells. However, present NAs are failed to eliminate cccDNA completely (Fontana, 2009; Toyama et al., 2019; Zoulim & Locarnini, 2009). For all these reasons, WHO has called for an active search for novel hits having greater efficacy, lower risk, and easy accessibility. The vast repertoire of bioactive phytoconstituents present in medicinal plants used in various traditional/folklore medicinal practices serves as an ideal repository for such purposes and is yet to be completely explored.

An improved understanding of the HBV lifecycle has made it easier for researchers to identify potential antiviral agents against the protein targets. HBV is a hepatotropic DNA virus (*hepadnaviridae* family) with a circular, double-stranded genome (~3.2 kb) with an envelope surrounding viral capsid, and replicates through reverse transcription of an RNA intermediate (pregenomic (pg) RNA) (Datta et al., 2012). HBV enters the host cell *via* the sodium taurocholate co-transporting polypeptide (NTCP) hepatocyte receptor (Herrscher et al., 2020). Upon entry of nucleocapsid into the cell, partly double-stranded relaxed circular DNA (rcDNA) gets transported into the nucleus and further gets converted into an episomal cccDNA, which is accumulated into a mini-chromosome (Guo et al., 2007). This cccDNA serves as the template for the transcription of viral mRNAs, resulting in the synthesis of the viral proteins (Guo et al., 2007; Liang, 2009). DNA polymerase binds to the epsilon domain (stem-loop structure) within the 5′ region of pgRNA and initiates its packaging into nucleocapsids (Tsukuda & Watashi, 2020). Here, the pgRNA is reverse transcribed to progeny rcDNA. Further, rcDNA gets enveloped and secreted out of the cell as virion particles (Tsukuda & Watashi, 2020). Thus, the formation and intracellular amplification of cccDNA through DNA polymerase plays a vital role in the establishment and maintenance of infection (Tsukuda & Watashi, 2020; Seeger & Mason, 2015). The conserved tyrosine–methionine–aspartate–aspartate (YMDD) active site of HBV-RT is necessary for polymerase activity and catalyses DNA synthesis, as well as essential for protein priming (Jones & Hu, 2013). Using the YMDD polymerase active site, the HBV DNA Pol—epsilon (H) complex starts protein priming by adding a single dGMP residue to Y63 of the TP domain (Jones & Hu, 2013).

Traditional/folk medicines have received considerable attention for the treatment of chronic infections and several drugs have been either discovered or derived from such natural products. Phytocompounds have been found responsible for diverse pharmacological actions, leading to the up and down-regulation of various proteins of interest, modulation of physiological functions, and host immune responses against infection (Adhikari et al., 2020; Dhama et al., 2013). Western Ghats of India is a biodiversity hotspot and is home to hundreds of medicinal plants, many of which are utilized for the treatment of conditions such as jaundice, liver disease, GI disorders, and viral infections like illness by folk healers/traditional practitioners without knowing much about their etiology. Traditional medicines are often considered to have less toxic effects compared to conventional drugs (Karimi et al., 2015). The screening of bioactive compounds from individual plants by experimental methods are highly demanding in terms of time and resources. Therefore, in the present study, we screened a library of phytocompounds from potential shortlisted herbs and virtually screened against modelled HBV-RT and also performed molecular pathway enrichment analysis of the identified potential hit,

in order to infer the affinity with host targets involved in the modulation of hepatitis B viral pathogenesis. Further, the effect of *in silico* identified plants extracts/enriched fraction/pure compound along with standard drug tenofovir disoproxil fumarate (TDF) effect on reverse transcriptase, cytotoxicity, time-dependent HBsAg and HBeAg secretion and intracellular HBV DNA, and pgRNA in HBV producing HepG2.2.15 cell line was measured. The gene set enrichment and network pharmacology analysis clearly inferred the pathways that corroborate with previous reports on selected medicinal plants to combat HBV induced HCC *via* RT inhibition and host immunomodulation. Thus, based on the current study findings, *Terminalia chebula* can be utilized as natural resource for the inhibition of HBV-RT and as a potential chemopreventive agent to combat liver cancer and HBV infection.

2. Material and methods

2.1. Computational pharmacology

2.1.1. Modelling of HBV-RT by fold recognition

Phyre2 based fold recognition was used to model the complete structure of HBV-RT (Kelley et al., 2015). To start with, the sequence of HBV-RT was retrieved from the UniProtKB database (ID: P03156; HBV genotype D; RT region aa 336-679) and submitted to the Phyre2 server for modeling. Further, based on heuristics method, the Phyre2 server utilized 6 HIV-RT template models [3kk1_B, 5dmq_A, 1rth_A, 2zd1_A, 2opq_A, and 1mu2_A] to generate a model of HBV-RT protein at >90% confidence in order to maximize trust, percentage identification, and alignment coverage.

In order to increase stereochemical efficiency, bonds, angles, and torsion angles to within statistically acceptable range, and side-chain refinement, the Phyre2 model structure was refined by two servers (1) locPREFMD (local Protein structure REFinement *via* Molecular Dynamics) (Feig, 2016) (2) GalaxyREFINE (http://galaxy.seoklab.org/cgi-bin/submit.cgi?type=REFINE) (Heo et al., 2013). The modeled HBV-RT structure was initially submitted to locPREFMD followed by GalaxyREFINE web server.

2.1.2. Loop modeling

The structure of the YMDD motif (Y203, M204, D205, D206 motif) of the HBV-RT plays a key role in protein priming (annotated as a structurally conserved loop based on the template (PDB id: 3kk1) used by Phyre2). Considering the root mean square deviation (RMSD) between model and template, HBV-RT conformation of YMDD loop was remodeled using ModLoop (https://modbase.compbio.ucsf.edu/modloop/) (Fiser & Sali, 2003). Further, RMSD between model and template was re-assessed in PyMOL (DeLano, 2002).

2.1.3. Lowest potential energy conformation by MD simulation

The lowest potential energy (PE) conformation was obtained by performing MD simulation (100 ns) using Desmond 6.1v (Bowers et al., 2006). The system was solvated in a cubical box of 10 Å x 10 Å x 10 Å periodic boundary conditions using the simple point charge (SPC) water model. The system was neutralised by adding 21 Cl^- counter ions. Water molecule geometry, bond distances, and bond angles of heavy atoms were restrained using the SHAKE algorithm. Particle mesh Ewald method was applied to calculate long-range interactions among the molecules. The Lennard-Jones interactions cut-off was set to 10.0 Å. The system was minimized for a 100 ps simulation run. NPT ensemble was used, wherein, "Nose-Hoover chain" Thermostat method with 1.0 ps relaxation time and the Barostat "Martyana-Tobias-Klein" method (with 2.0 ps relaxation time) were used to maintain pressure and temperature to 1 bar and 300 K, respectively. The Coulombic short-range cut-off radius was set to 9.0 Å. Finally, the lowest PE conformation was retrieved from the 100 ns of production run.

The coordinates of the catalytic Mg^{2+} and known inhibitor were assigned from the template to the refined lowest potential energy conformation using Modeller *ver* 10.0 with copy-ligand.py script of modeller. A total of 100 models were generated using modeller, among these, the model with the lowest discrete optimized protein energy (DOPE) score model was selected for further docking studies.

2.1.4. Documentation and mining of phytocompounds

Traditional herbal medicines, which are in practice with local/tribal healers in North Karnataka, India, and also as per documentation in the literature were identified based on essential criteria like claimed efficacies in treating jaundice, fever, inflammation, and liver infection. Plants that are rare, endangered, and not easily available in the Western Ghats were not considered. Phytocompounds from selected plants were retrieved from the Database of Ethnomedicinal Plants of Western Ghats (Vinayak et al., 2010) (https://nitmmed-plantsdb.in/), Dr. Duke's Phytochemical and Ethnobotanical Databases, PhytoChemical Interactions DB (PCIDB; https://www.genome.jp/db/pcidb/), and public repositories. The list of plants and their phytocompounds with references were provided in Supplementary Table 1.

2.1.5. Docking studies

Docking of known inhibitor ligand was performed with HBV-RT (control docking) using AutoDock vina *via* executing through the POAP pipeline (Samdani & Vetrivel, 2018) to re-confirm and validate the ligand-binding site. The grid box was set at the ligand-binding site having grid centre $x = 35.969$, $y = 79.743$, $z = 27.288$ Å [size $x = 18.985$ Å, $y = 24.983$ Å, $z = 20.812$ Å] with grid spacing and exhaustiveness 1 Å and 100, respectively. Atomic-level detailed intermolecular interactions between HBV-RT, native ligand, and Mg^{2+} cation were explored using Discovery Studio Visualizer ver 2019 (DSV v2019). The structural similarity between the standard molecule model and docking conformation was analysed by DSV v2019 (value 1 indicates the exact match or similar).

Following the docking of the known inhibitor (control) virtual screening was performed using a library of phytochemicals with HBV-RT utilizing the same grid dimensions and docking

parameters used for control docking. Finally, the Intermolecular interactions of the potential inhibitors were investigated using the Discovery studio visualizer.

2.1.6. Structural stability of docked complexes

The structural stability of HBV-RT with catalytic Mg^{2+} (RT-Mg^{2+}), HBV-RT complexed with known HIV-RT inhibitor modelled as per PDB ID: 3KK1 [(2R,5R)-5-(6-aminopurin-9-yl)-4-fluoro-2,5-dihydrofuran-2-yl]oxymethyl-[hydroxy(phosphonooxy)phosphoryl]oxy-phosphinic acid (RT-Mg^{2+}-Std), HBV-RT-Mg^{2+}-Std re-docked complex, and HBV-RT-Mg^{2+} with top screened phytocompounds (15 complexes) with lower BE and higher number of intermolecular interactions with the active site than the known inhibitor were validated by MD simulation for 100 ns using Desmond 6.1v. The parameters used for explicit MD simulation were adopted from similar studies documented earlier (Patil et al., 2021, 2022; Umashankar et al., 2021). Finally, the MD trajectories were analyzed using the in-build Desmond Protein-Ligand interactions module. The root mean square deviation (RMSD) values of the protein backbone and protein-ligand complexes, root mean square of fluctuation (RMSF) of residues were analyzed as validation parameters.

2.1.7. Prime MM-GBSA

Schrödinger Prime MM-GBSA module was used to calculate the relative binding-free energy (ΔG bind) of screened phytochemicals with HBV-RT using the equation $\Delta G_{GB} = \Delta E_{MM} + \Delta G_{solv} + \Delta G_{SA}$. The ΔG_{GB} represents the electrostatic solvation energy. ΔE_{MM} is "the difference between the minimized energies of the protein-ligand complex and the total energies of the protein and ligand in free form". ΔG_{solv} is "the difference in the GBSA solvation energies of the protein-ligand complex and the sum of the solvation energies of protein and ligand in free form". ΔG_{SA} is "the difference in the surface area energies for an unbound form of protein and ligand". The final frame of the MD simulation was used to estimate the binding free energy in all the cases. The parameters used for MM-GBSA are based on earlier similar studies (John et al., 2017; Muralikumar et al., 2017).

2.1.8. Gene set enrichment analysis and network construction

The phytocompounds–regulated host protein targets were predicted from the experimentally determined protein-ligand interaction database (BindingDB), wherein the search cutoff was set at Pa $\geq$ 0.7. STRING and KEGG pathway databases were used to trace the phytocompounds–modulated molecular pathways which were further integrated into phytocompounds-targets-pathways interaction map using Cytoscape (Shannon et al., 2003) (https://cytoscape.org/) *ver.* 3.6.1. During the network construction process, the topological parameter "edge count" was applied for mapping node color and size from low to high (Khanal et al., 2022; Patil et al., 2020).

2.1.9. Prediction of drug-likeness and biological spectrum

Canonical SMILES of each compound were submitted to molsoft (http://molsoft.com/) in order to predict the drug-likeness score (Patil et al., 2021). The biological spectrum of each phytocompound was retrieved using canonical SMILES by querying at PASS (prediction of activity spectra for substances) (Stepanchikova et al., 2003) online server (http://www.way2drug.com/passonline/). Pharmacological activity (Pa) score $\geq$0.3 was considered and from the prediction, hepatoprotectant, hepatic disorders treatment, and antiviral activities were traced.

2.2. In vitro *pharmacology*

2.2.1. Collection of plant material, their authentication, and procurement of pure compound

Based on the *in silico* findings, *Terminalia chebula*, *Bidens pilosa*, and *Centella asiatica* plants were prioritized and were collected from the local area of Belagavi, Karnataka, India, identified and certified by a qualified plant taxonomist at ICMR-NITM, Belagavi. The voucher specimen of the same has been deposited in ICMR-NITM with accession numbers RMRC-1639, RMRC-1640, and RMRC-1641, respectively for future reference. 1,2,3,4,6-penta-O-galloyl-β-D-glucose (PGG, CAS No. 14937-32-7; G7548) and standard compound Tenofovir Disoproxil Fumarate (TDF, CAS No. 202138-50-9; SML1794) were purchased from Sigma, USA.

2.2.2. LC-MS analysis

T. chebula n-butanol fraction, water extract, *B. pilosa* hydroalcoholic extract, and *C. asiatica* methanolic extract were subjected to LC-MS analysis (These extracts/fraction are reported to contain *in silico* identified compounds). The following conditions were maintained in running the sample on LC-MS ((a) UPLC Make: Waters, USA and Model: Acquity UPLC; (b) MS Make: Waters, USA and Model: Xevo G2-XS QTof). The C18 column (Accucore C18, 50 × 4.6, 2.6 u) was used as a stationary phase. Mobile Phase-A: 0.1% Formic acid in water and Mobile Phase-B: Acetonitrile was used. Capillary Voltage: 3.0KV, Collision Energy: 20 V, Ramp Collision Energy: 30-90 V, Source Temp: 150 °C, Desolvation Temp: 450 °C, Cone gas: 50 L/Hr, Desolvation Gas Flow: 800 L/Hr parameters were used. The extract was dissolved in the mobile phase and injected (volume 5 μL).

2.2.3. In vitro *cytotoxicity assay*

2.2.3.1. Procurement of HepG2.2.15 cell lines and maintenance. Hepatitis B Virus expressing HepG2.2.15 cell line (a subclone of HepG2 human hepatoblastoma that stably expresses the HBV) was kindly obtained from the International Centre for Genetic Engineering and Biotechnology (ICGEB) after approvals from the Institutional Biosafety Committee (IBSC) (IBKP TAI No. C100753). The cells were cultured in Dulbecco's Modified Eagle's Medium (DMEM) supplemented with 10% fetal bovine serum (FBS) with suitable antibiotics (G418). The cells were sub-cultured and maintained until they reached ~70%

confluence in T25 flasks at 37 °C with 5% CO_2 in a humidified incubator.

2.2.3.2. Preparation of test samples. Based on the in silico study, *T. chebula* n butanol fraction (TCN), water extract (TCW), *B. pilosa* methanolic (BPM) and hydroalcoholic extract (BPHA), and *C. asiatica* hydroalcoholic extract (CAHA) were subjected to *in vitro* studies. Initially, 10 mg/mL stock concentration of the samples were prepared in 5% DMSO in sterile water and filtered using a 0.22 μM syringe filter. From stock, different concentrations (15.65–2000 μg/mL) for extracts and fraction and 15.62 to 250 μM for PGG and TDF were prepared in DMEM and used for MTT assay.

2.2.3.3. MTT assay in HepG2.2.15 cell line. The cytotoxic activity of the above samples were tested on HepG2.2.15 cell line and CC_{50} was determined using MTT assay (Patil, Patil, et al., 2022). 20,000 cells/well were seeded onto 96-well flat-bottom plates and were allowed to grow for 24 h. Then the cells were treated with different concentration of samples and the final volume in each well was made up to 250 μL with DMEM media supplemented with 2% FBS and incubated for 24 h, at 37 °C in 5% CO_2. Further, the wells were washed with PBS, and added 20 μL of MTT reagent (5 mg/mL stock) to all the wells and incubated for 4h at 37 °C in 5% CO_2. After incubation, the wells were washed with PBS thrice to remove the MTT. The MTT reduction product (formazan crystals) was then dissolved in 100 μL of 99.5% DMSO by gentle shaking and the absorbance was noted at 570 nm using an UV-Vis spectrophotometer. The cytotoxic activity was expressed as a percentage cell viability and CC_{50} concentrations were determined from linear regression curve.

$$\%\ Cell\ viability = \frac{Absorbance\ of\ control - Absorbance\ of\ sample}{Absorbance\ of\ control} \times 100$$

2.2.4. Reverse transcriptase inhibitory assay

The reverse transcriptase inhibitory assay of TCN, TCW, BPM, BPHA, CAHA, PGG, and TDF were carried out using a manufacturer's protocol (Sigma Aldrich, USA; SKU No. 11468120910). The detailed protocol was provided in Supplementary document 1. The percentage RT inhibition is calculated as

$$\%\ RT\ Inhibition = \frac{Absorbance\ of\ control - Absorbance\ of\ sample}{Absorbance\ of\ control} \times 100$$

2.2.5. Relative quantification of intracellular HBV DNA and pgRNA by qRT-PCR

The genomic DNA free nucleic acid (Total RNA and viral DNA) was extracted from cells using RNeasy plus mini kit (Quiagen, Cat No. 74004) following the manufacturer's protocol. The extracted genomic free nucleic acid was quantified using Nanodrop (MAChine). cDNAs were synthesized using 200 ng of genomic-free nucleic acid using PrimeScript RT Reagent Kit (DSS Takara Bio India, Cat No. RR037A) as per the manufacturer's protocol. The relative expression of pgRNA of HBV in each sample was quantified by real-time qPCR using SYBR green PCR Master Mix (DSS Takara Bio India; Cat No. RR820A) using primers HBVR-F: GAGTGTGGAT TCGCACTCC, HBVR-R: GAGGCGAGGGAGTTCTTCT. Further, the HBV DNA from each sample was quantified using specific primers: HBVD-F: GTTGCCCGTTTGTCCTCTAATTC, HBVD-R: GGAGGGATACATAGAGGTTCCTTGA. RT PCR amplifications were performed on BIORAD CFX Maestro (Version 1.1). Cycle conditions were 95 °C for 30 s, followed by 40 cycles at 95 °C for 5 s and 60 °C for 30s. mRNA expression was analyzed using the ΔΔCT method and normalized with respect to the expression of the beta-actin. Amplification of specific transcripts was further confirmed by obtaining dissociation (melting) curve profiles with 1 cycle from 60 to 95 °C at an increment of 0.5 °C for 0.05s.

2.2.6. Time-course analysis of HBsAg and HBeAg

The cells were treated with different concentrations of test drugs for 5 days. The level of HBsAg was measured on 24, 48, 72, 96, and 120h, and HBeAg was measured on 24, 72, and 120h in the culture medium using an ELISA kit according to the manufacturer's instructions [(HBsAg Hepalisa kit was purchased from J. Mitra & Co. Pvt. Ltd, Cat No. IR020096) and (HBeAg Kit was purchased from Bioneovan Co. Ltd, Cat No. BE103A)]. The detailed protocol was provided in Supplementary document 1. The percentage HBsAg and HBeAg inhibition is calculated as

$$\%\ Inhibition = \frac{Absorbance\ of\ control - Absorbance\ of\ sample}{Absorbance\ of\ control} \times 100$$

2.3. Statistical analysis

The network was analyzed by the "Edge count" topological parameter. The docking score and binding free energy score was represented in kcal/mol unit. MTT assay data were represented in % cell viability and CC_{50} value. RT inhibition data were expressed as % inhibition and IC_{50}. HBsAg and HBeAg levels are represented as % inhibition. The mRNA expression was analyzed using the relative fold change using ΔΔCT method.

3. Results

3.1. Homology modelling

The HBV-RT structure obtained from Phyre2 server showed a confidence score of >90% for 85% residues (total number of residues 343) of HBV-RT. Phyre2 used 6 HIV RT templates: 5dmq, 3kk1, 1rth, 2zd1, 2opq, and 1mu2 to model the structure of HBV-RT based on heuristics in order to maximize confidence, percentage identity, and alignment coverage. Further, the modelled structure was subjected to structural refinement using locPREFMD with a total score of 1.302 (goal <1.0). Subsequently, the GalaxyRefine server was used to obtain an energetically favourable state (total 5) of the

modeled HBV-RT structure. Using the stereochemical properties we choose the model with better fitment in to the Ramachandran plot (~97% in the allowed and favoured region) and a significant ERRAT quality score (71.296%) has proceeded for further analysis.

3.2. Least potential energy conformation by MD simulation

The structural stability of the refined HBV-RT model was analyzed by performing all atom-explicit MD simulations for 100 ns. The least PE conformation (-150060.689 kcal/mol) was obtained at 89247ps.

3.3. Stereochemical properties of modeled HBV-RT

The refined HBV-RT model characteristics were analyzed by PROCHECK and ERRAT sever (Supplementary Figure S1). The overall quality factor of HBV-RT model was found to be 75.09%. About 98.7% (including YMDD motif) were found within the favoured region and 0% residues were found in the additionally allowed region. Among the total 343 residues, 298 were non-glycine and non-proline residues, 2 were end residues, 21 were glycine residues, and 23 were proline residues.

3.4. Structural similarity of HBV-RT

We optimized the geometry of YMDD motif (active site) using ModLoop by considering the structural similarities with the template structures. The HBV-RT and 3kk1 showed a structural similarity of 4.520 Å (Supplementary Figure S2(a)). The active site residues from the "YMDD motif; Y203, M204, D205, D206" showed maximum structural similarities with the template 3kk1 (RMSD= 0.586 Å) (Supplementary Figure S2(b)). Further, the structural analysis of HBV-RT (UniProt ID P03156) revealed that the two catalytic Mg^{2+} ions are stabilized by the catalytic triads formed by the residues "Asp83, Asp205, and AspD206" which are crucial for the enzymatic activity. Among the 6 templates used, only 3kk1 was found to contain Mg^{2+} and known HIV RT inhibitor bound to the active site. In 3kk1, catalytic Mg^{2+} formed covalent bond interaction with "Asp110, Asp185, and Asp186" catalytic triad residues. Therefore, we used 3kk1 as a structural modelling the ligands in HBV-RT model.

3.5. Metal ion and native ligand transfer

In the modelled "HBV-RT-Mg^{+2} in complex with known inhibitor", the Mg^{2+} ion formed 5 co-ordination bonds with Asp83 (2.56 Å), Asp83 (2.75 Å), Val84 (2.23 Å), Ser85 (3.0 Å), Asp205 (2.26 Å), and known inhibitor formed one hydrophobic interaction, i.e. Phe88 (2.94 Å), six hydrogen bonds, i.e. Arg41 (2.18 Å), Asp83 (3.40 Å), Ala87 (1.97 Å), Asn236 (2.94 Å), Lys239 (2.97 Å), Lys239 (2.65 Å), one halogen bond Met171 (3.68 Å), and three salt bridges, i.e. Arg41 (4.41 Å), Arg41 (4.22 Å), and Lys239 (4.0 Å). Figure 1 and Supplementary Figure S3 show the Mg^{2+} ion and known inhibitor interactions with an active site residue of HBV-RT.

3.6. Docking validation

Docked complex of HBV-RT with known inhibitor showed a binding energy of −8.0 kcal/mol. The Mg^{2+} formed 5 co-ordination bonds with Asp83 (2.56 Å), Asp83 (2.75 Å), Val84 (2.23 Å), Ser85 (3.0 Å), Asp205 (2.26 Å) and ligand 914 formed five hydrogen bonds, i.e. Arg41 (2.13 Å), Asp83 (3.13 Å), Arg41 (3.57 Å), Asp83 (3.71 Å), Lys239 (2.84 Å), one pi-cation interaction with Arg41 (3.78 Å), and three salt bridges, i.e. Arg41 (3.79 Å), Arg242 (5.24 Å), and Lys239 (5.36 Å). The structural superimposition of the docked conformation and the template showed the RMSD value of 0.7499 Å (Supplementary Figure S4).

3.7. Docking of phytocompound with HBV-RT

The virtual screening of 268 phytocompounds resulted in the top 15 molecules namely, 1,2,3,4,6-penta-O-galloyl-e-D-glucose

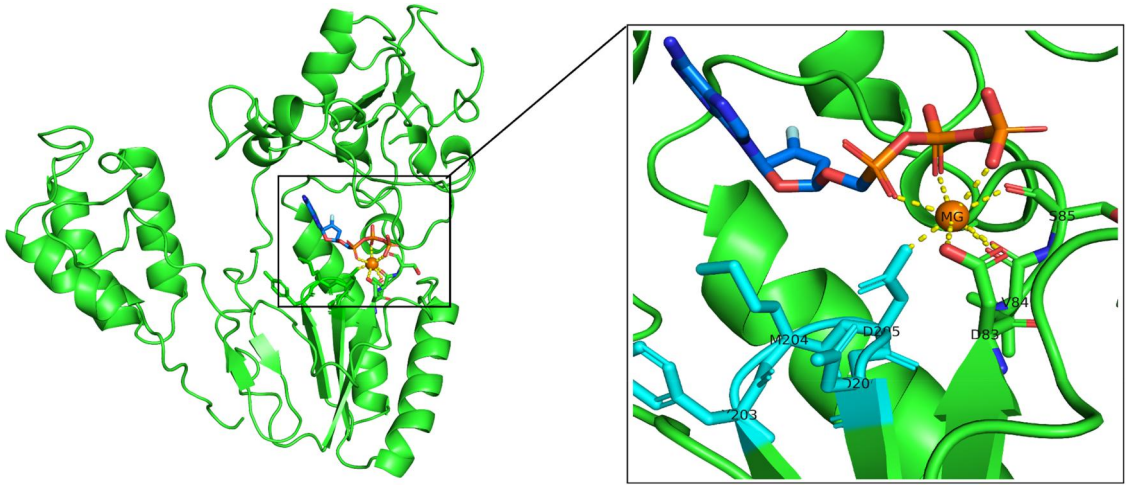

Figure 1. Interaction of Mg^{2+} ion and standard molecule with HBV RT. The Mg^{2+} ion formed the Mg formed 8 co-ordination bond (3 with standard molecule and 5 with the HBV RT).

(BE −8.1 kcal/mol), Chebulagic acid (BE −8.5 kcal/mol), Tellimagrandin I (BE −9.1 kcal/mol), 1,3,6-Tri-O-galloyl-β-D-glucose (BE −9.3 kcal/mol), 2,3,4,6 tetra-O-galloyl-β-D-glucose (BE −8.6 kcal/mol), Terflavin-C (BE −9.4 kcal/mol) from *Terminalia chebula*; Okanin (BE −7.2 kcal/mol), Centaurein (BE −7.9 kcal/mol), Okanin-4′-O-glucoside (Marein) (BE −7.8 kcal/mol), Jacein (BE −8.5 kcal/mol), Okanin 4-methyl ether 3′-glucoside (BE −7.5 kcal/mol) from *Bidens pilosa*; Delphinidin 3-O-glucosyl-glucoside (BE −8.6 kcal/mol), Isorhamnetin 3-O-rutinoside (BE −8.2 kcal/mol), Delphinidin 3,5-O-diglucoside (BE −8.2 kcal/mol), Castillicetin (BE −8.2 kcal/mol) from *Centella asiatica* were identified as potential inhibitors of HBV-RT. All these 15 hits showed significant intermolecular interactions with YMDD and RT1 motif residues which are conserved in the template structure. Table 1 and Supplementary Table 2 represent the BE and interactions of prioritized and overall screened phytocompounds with HBV-RT, respectively.

3.8. Structural stability of docked complexes

The structural stability is mainly characterized by the RMSD and RMSF trajectories of MD simulation, here we analyzed RMSD of the backbone, protein-ligand complex, and RMSF (C-alpha) of a standard molecule, as well as selected phytocompounds (15) complexed with HBV-RT (refer Figure 2, Figure 3, and Figure 4), respectively.

3.8.1. Stability of HBV-RT – Mg^{2+} – Std model

Initially, the protein backbone exhibited a stable RMSD within ∼4.0 Å to 5.8 Å from 0 ns to ∼35 ns and was found to attain more stability from 35 ns to 100 ns, wherein it tends to sustain within 5.5 Å to 6.4 Å. Similarly, the protein-ligand complexes exhibited a stable RMSD from 0 ns to 35 ns with slight fluctuations. The complex RMSD showed significant variations (7.5 Å to 11 Å) initially, but further got stabilized at a higher RMSD of 11.0 Å. The C-terminal loop region showed maximum fluctuations due to the flexibility of terminal residues. The linker region formed between Leu311 and Ala320 connecting helices at the C-terminal also showed higher fluctuation >4 Å (Supplementary Movie 1). The active site residues namely Asp83, Val84, Ser85, Tyr203, Met204, Asp205, and Asp206 showed the least fluctuations (∼1.5 Å), as these residues form stable contacts with Mg^{2+} and the ligand. The complex intermolecular interaction analysis that that Mg^{2+} to form a very stable (100%) interaction fraction with Asp83, Val84, Ser85, and Asp205. Whereas, with ligand, Tyr245 and Asn248 formed a stable hydrophobic interaction for around 22% and 37%, respectively. Moreover, Glu39, Arg41, Ala86, Tyr245, Asn245, and Gln262 were found to be involved in the formation of hydrogen-bonded interactions.

3.8.2. Stability of HBV-RT-Mg^{2+} -Std docked complex

The HBV-RT—Mg^{2+}—Std docked complex showed an equilibration period of about 15 ns, further which it showed stable RMSD value ranging from ∼7.2 to 9 Å. A similar trend of RMSD was also observed in protein-ligand complex, but this complex got stabilized at relatively higher RMSD of 9.5 to 14.5 Å after the equilibration period of first 15 ns. Similar to the control complex, this re-docked complex also showed higher fluctuations mainly at the C-terminal loop region. The linker joining the two helices at the C-terminal (Leu311 to Ala320) showed higher fluctuation >5 Å (Supplementary Movie 2). The binding pocket residues Asp83, Val84, Ser85, Tyr203, Met204, Asp205, and Asp206 showed least fluctuations ∼2.0 Å, as these are actively engaged in forming stable interactions with Mg^{2+} and ligand. Asp205 and Asp206 residues formed stable H-bonded interactions for around 61% and 39%, respectively, and water bridge interactions for around 15% and 10%, respectively. Whereas, Arg41 and Lys239 formed water-bridge interaction for around 11% through the simulation. Supplementary Figure S5(a,b) shows the residue-wise contacts of standard molecule with HBV-RT.

3.8.3. Stability of HBV-RT-Mg^{2+}-phytocompound complexes

The top-ranking complexes having a significant binding affinity towards HBV-RT active site were selected and subjected for MD simulation for 100 ns. The MD simulation revealed 15 compounds from the plants *T. chebula* (6), *B. pilosa* (5), and *C. asiatica* (4) plants to show stable ligand-protein contacts, RMSD, and RMSF when compared to the standard molecule. Amongst these 15 complexes studied, considering the highest binding affinity, stable contacts, RMSD, and RMSF values, the HBV-RT – *1,2,3,4,6-penta-O-galloyl-β-D-glucose* complex (from *Terminalia chebula*) was found to be the top ranking and potential hit.

3.8.3.1. Stability of HBV-RT and 1,2,3,4,6-penta-O-galloyl-β-D-glucose complex. This complex featured higher stability in MD simulation when compared to all the other complexes, with RMSD value ranging between ∼4.0 Å to ∼8.6 Å. A steady increase in RMSD value from ∼4.0 Å to ∼7.5 Å was observed during the equilibration period of 0-20 ns, and further got stabilized at higher RMSD value (∼8.0 and 9.0 Å). Whereas, RMSD for whole protein-ligand complex shows relatively stable RMSD (∼4.8 Å to ∼6.0 Å) throughout the simulation. The C-terminal flexible loop shows fluctuations due to flexibility of terminal residues. The linker joining the two helixes at the C-terminal (Leu311 to Ala320) showed slight fluctuation >2 Å. Also, the loop region (Tyr148 to Lys152) showed minimal fluctuation ∼4 Å compared to other protein-ligand complexes. However, binding pocket residues Asp83, Val84, Ser85, Tyr203, Met204, Asp205, and Asp206 showed maximum residual fluctuations of ∼1.4 Å, as these are actively engaged in forming very stable interaction with Mg^{2+} and 1,2,3,4,6-penta-O-galloyl-β-D-glucose similar to known inhibitor (Supplementary Movie 3). The analysis of intermolecular interactions revealed that Asp205 to form a water-bridge for 24%, and hydrogen bond interactions for 53%, 34%, and 20% of the interaction fraction. Asp206 showed water-bridge formation (12%), and H-bonding interactions for 46%, 33%, and 21% of the interaction fraction. Arg41 forms water bridge for 34% and other residues viz., Ser40, Leu42, Ala87, Phe88, Gly172, Asn248, Phe249, Met250, Arg289, Gly292 formed water-bridge, hydrophobic and

Table 1. Binding energy and intermolecular interactions of phytocompounds with HBV-RT.

Plant name	Compound name	Class of compound	PubChem ID	Binding Energy (kcal/mol)	Hydrogen Bond interaction (No. of interactions)	Metal ion Mg^{2+} interaction after MD simulation (Yes/No)	Van der Waals, C-H, Pi-Cation, Pi-Anion, Amide-Pi stacked, Pi-Alkyl, Pi-Sigma
Terminalia chebula	1,2,3,4,6-penta-O-galloyl-β-D-glucose	Tannin	65238	−8.1	Val84, Ala87, Asp205 (2), Arg41, Lys239, Met171 (2)	Yes	Val43, Arg41, Ala87
Terminalia chebula	Terflavin-C	Tannin	101589227	−9.4	Lys239, Arg41 (2), Arg242, Asp206 (2), Asp205, Asn248 (2), Met250	Yes	Lys239 (3), Asp83, Pro34, Arg41, Asp205, Arg242, Met250
Terminalia chebula	Chebulagic acid	Tannin	250397	−8.5	Arg41 (2), Asp205, Arg242, Asn248 (2), Gln262	Yes	Met204
Terminalia chebula	2,3,4,6 tetra-O-galloyl-β-D-glucose	Tannin	101011018	−8.6	Arg41, Ala87, Ser85, Asn236, Lys239, Asp206 (2)	Yes	Met204, Phe88, Met171, Val30, Val43, Ala86, Ser85, Asp205 (2), Asp206
Terminalia chebula	1,3,6-Tri-O-galloyl-β-D-glucose	Tannin	452707	−9.3	Arg242, Asp206, Asp205 (2), Lys239, Val84, Ala87, Arg41 (2), Met171	Yes	Met171, Lys239
Terminalia chebula	Tellimagrandin I	Tannin	442690	−9.1	Val44 (2), Arg41, Val84, Ala87 (2), Asp205 (3), Asp206, Arg242, Lys239	Yes	Met204 (2), Ala87, Val43
Bidens pilosa	Okanin	Flavonoid	5281294	−7.2	Ser85, Arg41, Asp205	Yes	Val48, Val30, Met171
Bidens pilosa	Okanin-4′-O-glucoside (Marein)	Flavonoid	6441269	−7.8	Met171, Phe88, Ala87, Ser85, Lys239, Asp206 (2)	Yes	Met171, Phe88 (2), Arg41, Asp205
Bidens pilosa	Okanin 4-methyl ether 3′-glucoside	Flavonoid	14162682	−7.5	Arg41 (2), Val44, Arg242, Asp206, Asp83 (2), Asp205	No	Val43
Bidens pilosa	Centaurein	Flavonoid	5489090	−7.9	Asp205, Lys239, Arg242	Yes	Arg41, Phe249, Phe88, Met171
Bidens pilosa	Jacein	Flavonoid	44259819	−8.5	Asp31, Lys239, Arg41 (2), Asp206, Asp205	No	Ala86, Arg41 (2), Lys239, Asp31
Centella asiatica	Castillicetin	Flavonoid	102394640	−8.2	Asp206, Arg41, Asp83	Yes	Arg41, Asp205, Val43, Val30, Met171
Centella asiatica	Isorhamnetin 3-O-rutinoside	Flavonoid	5481663	−8.2	Asp31, Asn248, Asp205, Ala87, Phe88	Yes	Lys239, Asp206, Arg242 (3), Leu42, Met171
Centella asiatica	Delphinidin 3-O-glucosyl-glucoside	Flavonoid	5316496	−8.6	Arg41 (2), Met171, Arg242, Ser85, Val84, Ala87, Lys239, Asp205, Asp206, Asn248	No	Arg41, Ala87, Asp206
Centella asiatica	Delphinidin 3,5-O-diglucoside	Flavonoid	10100906	−8.2	Val44, Ala87, Arg41, Asp205, Asp206	No	Met171, Ser85, Val30 (2), Arg41 (2), Asp205, Met204
Standard inhibitor	[(2R,5R)-5-(6-aminopurin-9-yl)-4-fluoro-2,5- dihydrofuran-2-yl]oxymethyl-[hydroxy(phosphonooxy) phosphoryl]oxy-phosphinic acid	HIV RT Inhibitor from 3kk1 PDB	https://www.rcsb.org/ligand/914	−8.0	Phe88, Ala87, Arg41 (2), Lys239	Yes	Arg242 (2), Asp83, Asp206, Asp205, Lys239, Arg41

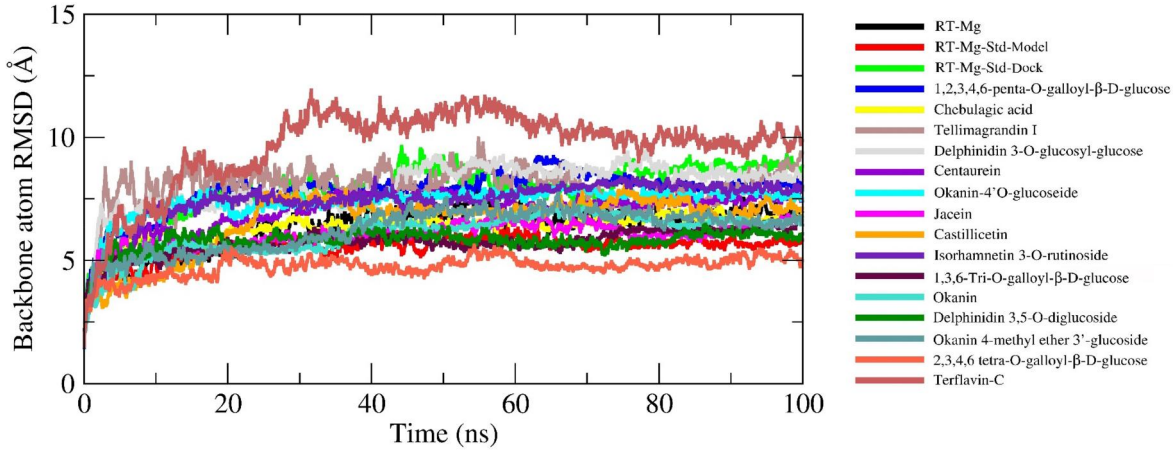

Figure 2. Protein backbone RMSD of HBV RT in complex with Mg^{2+} ion, standard molecule and phytocompounds.

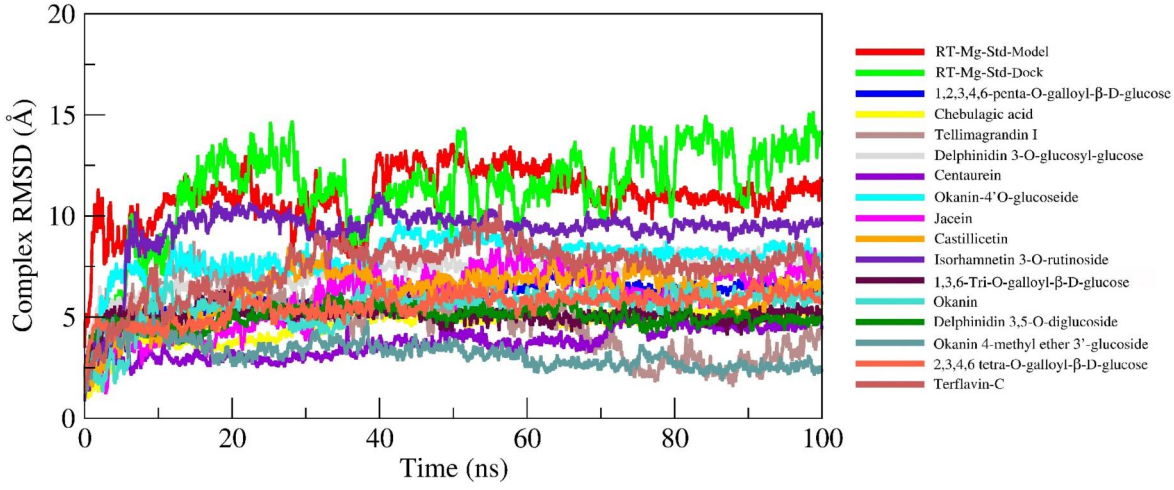

Figure 3. Complex RMSD of HBV RT in complex with Mg^{2+} ion, standard molecule, and phytocompounds.

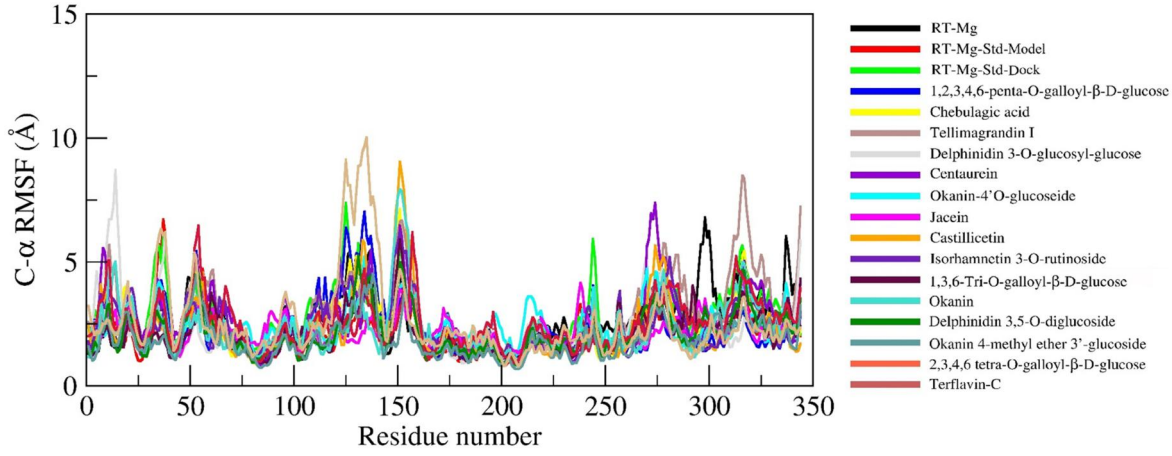

Figure 4. RMSF of HBV RT in complex with Mg^{2+} ion, Standard molecule, and phytocompounds.

hydrogen interactions with 1,2,3,4,6-penta-O-galloyl-β-D-glucose (refer Supplementary Figure S6(a,b)).

3.9. MM-GBSA calculation

Among the 15 complexes studied, 1,2,3,4,6-penta-O-galloyl-e-D-glucose scored the least free binding energy of −113.774 kcal/mol. Whereas, Okanin 4-methyl ether 3′-glucoside was found to be the second-ranked complex with the least free binding energy of −87.165 kcal/mol. These complexes showed significantly higher binding affinity towards HBV-RT when compared to its known inhibitors (RT-Mg^{2+}-Std model complex = −25.075 kcal/mol and RT-Mg^{2+}-Std-Docked complex = −11.069 kcal/mol). Table 2 describes the energy components estimated with prime MM-GBSA calculation.

3.10. Gene set enrichment and network analysis

Gene set enrichment analysis of 15 phytocompounds modulating 74 targets (Supplementary Table 3) were predicted to modulate 37 molecular pathways (Supplementary Table 4). Among these, 39 proteins were found to be involved in 15 molecular pathways (Supplementary Table 5) associated with HBV infection and its associated complications like HCC: Complement and coagulation cascades, Pathways in cancer, Steroid hormone biosynthesis, Tryptophan metabolism, MicroRNAs in cancer, HIF-1 signaling pathway, Calcium signaling pathway, Proteoglycans in cancer, Bile secretion, Transcriptional misregulation in cancer, Viral protein interaction with cytokine and cytokine receptor, NF-kappa B signaling pathway, Insulin resistance, Apoptosis, and mTOR signaling pathway. Among these 39 protein targets, TNF, PLAU, PTPN1, and MMP9 were identified as hub genes within the network as they scored edge count of 11, 9, 9, and 9, respectively (Figure 5).

3.11. Prediction of drug-likeness and biological spectrum

All the identified 15 phytocompounds were screened for their druggability using Molsoft server. Among all, 1,3,6-Tri-O-galloyl-β-D-glucose was predicted to possess the highest drug-likeness score (0.92) and Terflavin-C scored the least (0.05). Interestingly, all the phytocompounds scored positive DLS. The biological spectrum of 15 compounds were obtained from the PASS online server with Pa>0.3, in which 13 compounds (2 not predicted) were found to be hepatoprotectant and antiviral properties (Table 3).

3.12. LC-MS profile of fraction and extracts

LC-MS profile of *T. chebula* n-butanol fraction, *T. chebula* water extract, *B. pilosa*, and *C. asiatica* hydroalcoholic extracts were examined for active principles which were identified in molecular docking and dynamics studies. The identified compound's retention time with molecular weight is provided in Supplementary Table 6. The LC-MS positive and negative mode chromatograms of *T. chebula*, *B. pilosa*, and *C. asiatica* were provided in Supplementary Figure S7 and Figure S8, respectively.

3.13. Cytotoxicity assay

The MTT assay showed the CC_{50} of TCW (1048.43 µg/mL) to be higher than that of the TCN (853.354 µg/mL) in

Table 2. Prime MM-GBSA calculation of the HBV RT Phytocompounds last frame complexes.

Compound name	PubChem CID	ΔG Bind (kcal/mol)	ΔG Bind Coulomb	ΔG Bind Covalent	ΔG Bind Hbond	ΔG Bind Solv GB	ΔG Bind vdW
1,2,3,4,6-penta-O-galloyl-e-D-glucose	65238	−113.774	−55.649	2.943	−2.913	78.094	−85.004
Chebulagic acid	250397	−41.325	−273.990	9.770	−1.492	301.630	−52.452
Tellimagrandin I	442690	−49.798	−101.560	0.773	−1.650	148.192	−64.050
1,3,6-Tri-O-galloyl-β-D-glucose	452707	−28.760	−20.085	−2.028	−1.613	53.421	−41.834
Okanin	5281294	−37.892	−109.257	4.762	−1.158	126.926	−33.450
Delphinidin 3-O-glucosyl-glucoside	5316496	−53.087	−30.011	2.125	−2.372	58.958	−38.960
Isorhamnetin 3-O-rutinoside	5481663	−45.786	−22.371	7.223	−1.244	46.273	−47.676
Centaurein	5489090	−48.112	−51.000	8.306	−1.676	71.999	−49.091
Okanin-4′-O-glucoside (Marein)	6441269	−32.156	−16.680	6.381	−0.981	53.801	−42.894
Delphinidin 3,5-O-diglucoside	10100906	−46.600	−41.236	8.229	−1.266	71.358	−42.466
Okanin 4-methyl ether 3′-glucoside	14162682	−87.165	−49.590	7.105	−2.323	50.091	−55.394
Jacein	44259819	−26.640	−31.620	11.293	−0.470	62.269	−40.448
2,3,4,6 tetra-O-galloyl-β-D-glucose	101011018	−65.812	−154.591	8.371	−1.269	186.386	−62.583
Terflavin-C	101589227	−30.623	−213.339	11.213	−2.069	257.182	−50.176
Castillicetin	102394640	−34.733	−28.701	−1.388	−2.345	48.782	−26.827
RT-Mg_Std-Model	–	−25.075	−401.053	0.793	−0.542	403.698	−22.107
RT_Mg_Std_Dock	–	−11.069	−295.403	3.694	−0.741	306.669	−21.207

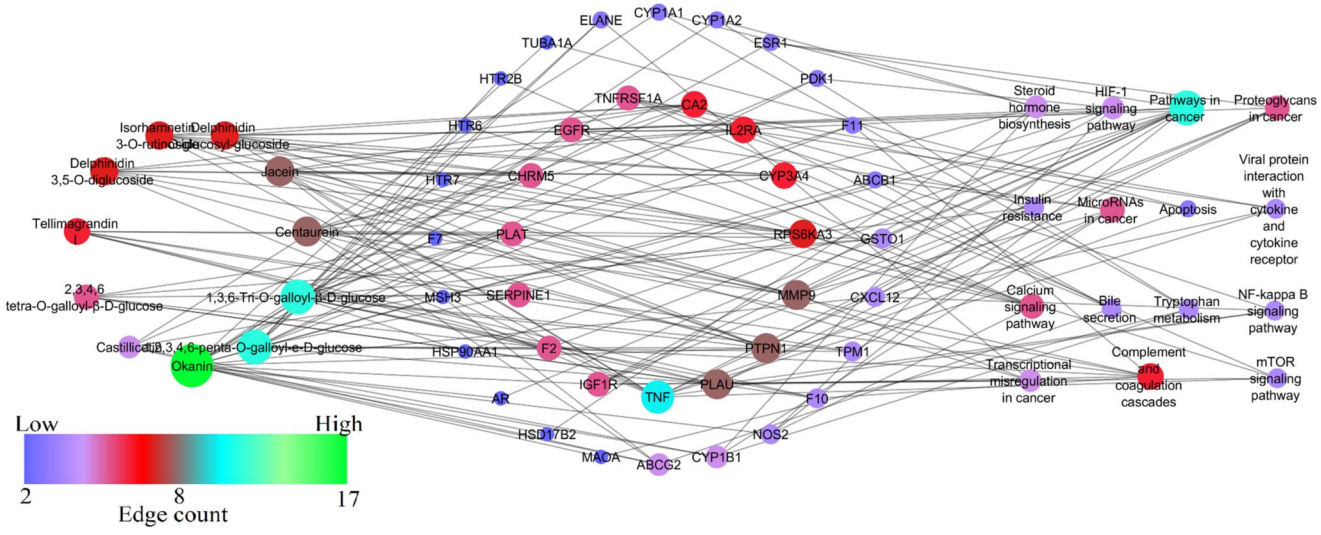

Figure 5. Network representation of phytocompounds, protein targets, and pathways.

Table 3. Phytocompounds druglikeness score and biological spectrum.

Plant name	Compound name	Druglikeness score	Activities confirmed (Pharmacological activity Pa > 0.3)
Bidens pilosa	Okanin	0.23	Antiviral (Influenza) (0.679), Hepatoprotectant (0.587), Hepatic disorders treatment (0.441), Antiviral (Herpes) (0.406), Antiviral (0.39), Antiviral (HIV) (0.322)
Bidens pilosa	Centaurein	0.71	Hepatoprotectant (0.972), Hepatic disorders treatment (0.672), Antiviral (Influenza) (0.56), Antiviral (Herpes) (0.495), Antiviral (Hepatitis B) (0.479)
Bidens pilosa	Okanin-4′-O-glucoside (Marein)	0.61	Hepatoprotectant (0.916), Antiviral (Influenza) (0.806), Hepatic disorders treatment (0.631), Antiviral (Herpes) (0.479), Antiviral (0.403), Antiviral (Hepatitis B) (0.402)
Bidens pilosa	Okanin 4-methyl ether 3′-glucoside	0.64	Hepatoprotectant (0.905), Antiviral (Influenza) (0.778), Hepatic disorders treatment (0.572), Antiviral (Herpes) (0.456), Antiviral (Hepatitis B) (0.356), Antiviral (0.338)
Bidens pilosa	Jacein	0.65	Hepatoprotectant (0.972), Antiviral (Influenza) (0.56), Antiviral (Herpes) (0.495), Antiviral (Hepatitis B) (0.479)
Centella asiatica	Delphinidin 3-O-glucosyl-glucoside	0.24	Not predicted: Molcharge: 1
Centella asiatica	Isorhamnetin 3-O-rutinoside	0.79	Hepatoprotectant (0.976), Antiviral (Influenza) (0.728), Hepatic disorders treatment (0.668), Antiviral (Herpes) (0.506), Antiviral (Hepatitis B) (0.428)
Centella asiatica	Delphinidin 3,5-O-diglucoside	0.67	Not predicted: Molcharge: 1
Centella asiatica	Castillicetin	0.65	Hepatoprotectant (0.8), Hepatic disorders treatment (0.545), Antiviral (Hepatitis B) (0.479), Antiviral (Herpes) (0.455), Antiviral (Influenza) (0.4)
Terminalia chebula	1,2,3,4,6-penta-O-galloyl-e-D-glucose	0.19	Hepatoprotectant (0.752), Antiviral (Herpes) (0.53), Antiviral (Influenza) (0.505), Hepatic disorders treatment (0.479), Antiviral (0.384), Antiviral (Rhinovirus) (0.336)
Terminalia chebula	Chebulagic acid	0.58	Hepatoprotectant (0.798), Antiviral (Herpes) (0.559), Hepatic disorders treatment (0.422), Antiviral (Hepatitis B) (0.348)
Terminalia chebula	Tellimagrandin I	0.3	Hepatoprotectant (0.884), Antiviral (Herpes) (0.668), Hepatic disorders treatment (0.581), Antiviral (Hepatitis B) (0.377), Antiviral (0.343)
Terminalia chebula	1,3,6-Tri-O-galloyl-β-D-glucose	0.92	Hepatoprotectant (0.783), Antiviral (Influenza) (0.676), Hepatic disorders treatment (0.557), Antiviral (Herpes) (0.513), Antiviral (0.411), Antiviral (Hepatitis B) (0.354), Antiviral (Rhinovirus) (0.348), Antiviral (Picornavirus) (0.305)
Terminalia chebula	2,3,4,6 tetra-O-galloyl-β-D-glucose	0.44	Hepatoprotectant (0.608), Antiviral (Rhinovirus) (0.595), Antiviral (Influenza) (0.509), Hepatic disorders treatment (0.424), Antiviral (0.33), Antiviral (Adenovirus) (0.345), Antiviral (Herpes) (0.318), Antiviral (Picornavirus) (0.303)
Terminalia chebula	Terflavin-C	0.05	Hepatoprotectant (0.973), Hepatic disorders treatment (0.759), Antiviral (Herpes) (0.567), Antiviral (Hepatitis B) (0.513), Antiviral (0.365)

HepG2.2.15 at 24h treatment. Similarly, the CC_{50} of BPM (1187.94 μg/mL) to be higher than that of the BPHA (615.558 μg/mL). The CC_{50} of CAHA was found to be 881.828 μg/mL and the CC_{50} of CAHA. PGG and TDF were found to be >250μM. Based on the MTT assay, ≤500μg/mL test concentration was used for TCN, TCW, BPHA, BPM, and CAHA and ≤250μM for PGA and TDF. Figure 6 and Supplementary Table 7 represent the concentration-dependent percentage viable cells and CC_{50} value for each test drug.

3.14. RT inhibitory assay

The reverse transcriptase (RT) colorimetric assay kit was used to test the test drugs RT inhibitory activity by *in vitro*. TCN and TCW potently inhibited the RT enzyme in a dose-dependent manner with an IC_{50} of 147.077 and 149.214 μg/mL, respectively. Whereas BPM, BPHA, and CAHA didn't show RT inhibitory activity, and the IC_{50} of BPM, BPHA, and CAHA was found to be 2056.25, 2000.955, and 1928.313 μg/mL, respectively. Similarly, PGG also showed RT inhibitory activity with IC_{50} of 149.075 μM and TDF, a standard molecule didn't show RT inhibitory activity at 250 μM concentration. The concentration-dependent % RT inhibition of each test drug was given in Figure 7 and Supplementary Table 8. Based on these findings, TCN, TCW, PGG, and TDF were prioritized for further studies as mentioned below.

3.15. Effect of TCN, TCW, PGG, and TDF on intracellular HBV DNA and pgRNA in HepG2.2.15 cell line

As Figure 8 shows, treatment of HepG2.2.15 cells with TCN 125, 250, and 500 μg/mL for 24h decreased the intracellular HBV DNA by 2^6 fold. Whereas, TCN 62.5 and 31.25 μg/mL decreased by 2^5 fold. Similarly, TCW 500 μg/mL showed 2^7 fold decrease in HBV DNA. TCW 250, 125, 62.5, and 31.25 μg/mL also showed 2^6, 2^6, 2^6, and 2^5 fold decreases in intracellular HBV DNA. PGG 100 μM showed about 2^5 fold decrease and PGG 50, 25, 12.5, and 6.25 μM showed about 2^3 fold decrease in HBV DNA. Whereas, TDF concentration range between 6.25 to 100 μM

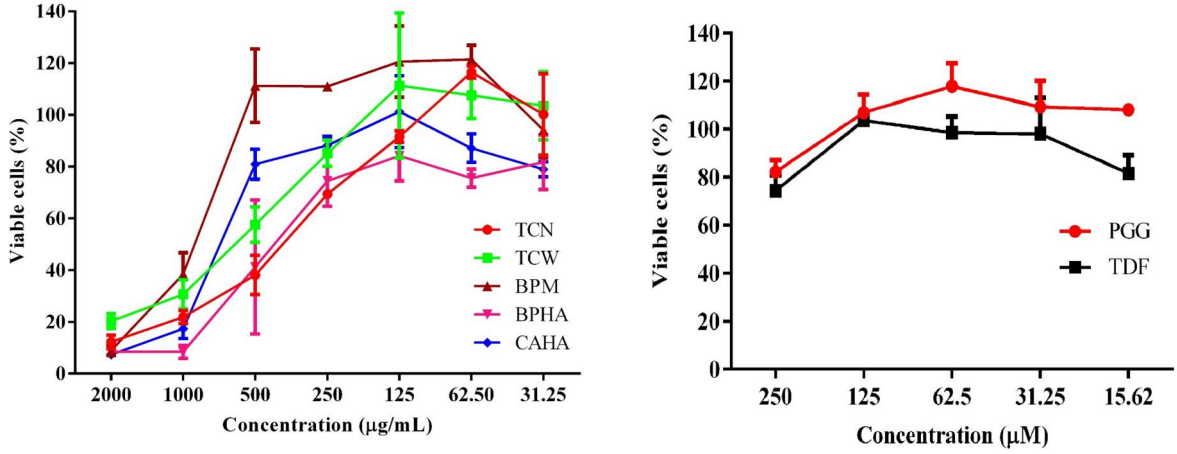

Figure 6. Cytotoxicity of extracts/fraction, PGG, and TDF in HepG2.2.15 cell line after 24h treatment. The results are expressed as the mean ± SEM of three independent biological replicates.

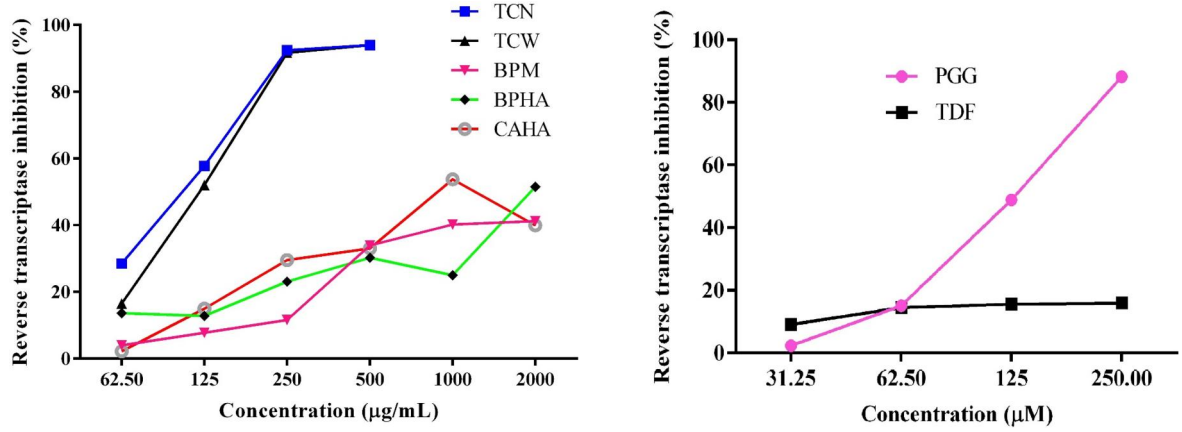

Figure 7. Effect of extracts/fraction, PGG, and TDF on RT enzyme.

showed about 2^1–2^2 fold decrease in intracellular HBV DNA. On looking into the pgRNA level, only TCN and TCW 500 µg/mL, and PGG 100 µM showed about 2^2 fold decrease in the pgRNA. This indicates TCN, TCW, and PGG to have a significant effect on intracellular HBV DNA but not on pgRNA.

3.16. Time-course analysis of HBsAg

The % inhibition of HBsAg secretion in the cell supernatant was analyzed at different time intervals (24, 48, 72, 96, and 120h). All the test drugs exhibited strong HBsAg inhibitory activity. At 24 and 48h, only TCN500 showed about 80% inhibitory effect and at 72, 96, and 120h TCN500 (∼85%), TCN250 (∼80%) and TCN125 (∼75%) exhibited an inhibitory effect. Interestingly, a similar effect was observed for TCW. Whereas, PGG100 showed ∼80% inhibitory effect at 96h and ∼70% at 120h. A standard compound TDF concentration TDF100 also showed ∼80% inhibitory effect at 96 and 120h. Figure 9 and Supplementary Table 9 represent the HBsAg inhibitory effect of TCN, TCW, PGG, and TDF.

3.17. Time-course analysis of HBeAg

The % inhibition of HBeAg secretion in the cell supernatant was analysed at different time interval (24, 72, and 120h). Among the selected test drugs, TCN and TCW exhibited strong HBeAg inhibitory activity. At 24h TCN500 showed about 80% inhibitory effect and at 72 and 120h showed about ∼72% and 60%. A similar effect was also observed for TCW. Whereas, PGG100 and TDF100 exhibited ∼43% and ∼20% inhibition, respectively. At 72 and 120h, a decrease in the inhibitory effect of HBeAg secretion was observed for all the test drugs. Figure 10 and Supplementary Table 10 represent the HBeAg inhibitory effect of TCN, TCW, PGG, and TDF.

4. Discussion

The present study aimed to model the HBV-RT protein structure in complex with Mg^{2+} ion and to infer the binding mode of known inhibitor, and to identify the druggable hit molecules against YMDD and RT1 motif of HBV-RT from traditional medicinal plants of the Western Ghats region of Karnataka, through the integration of series of chemoinformatics tools, i.e. homology modelling, molecular docking and dynamics, MM-GBSA calculation, gene set enrichment, and network pharmacology. It was also aimed to identify biological spectra of the prioritized molecules for their hepatoprotective and antiviral efficacy through PASS server prediction. To validate the *in silico* findings, *T. chebula* n butanol fraction (TCN) and water extract (TCW), *B. pilosa*

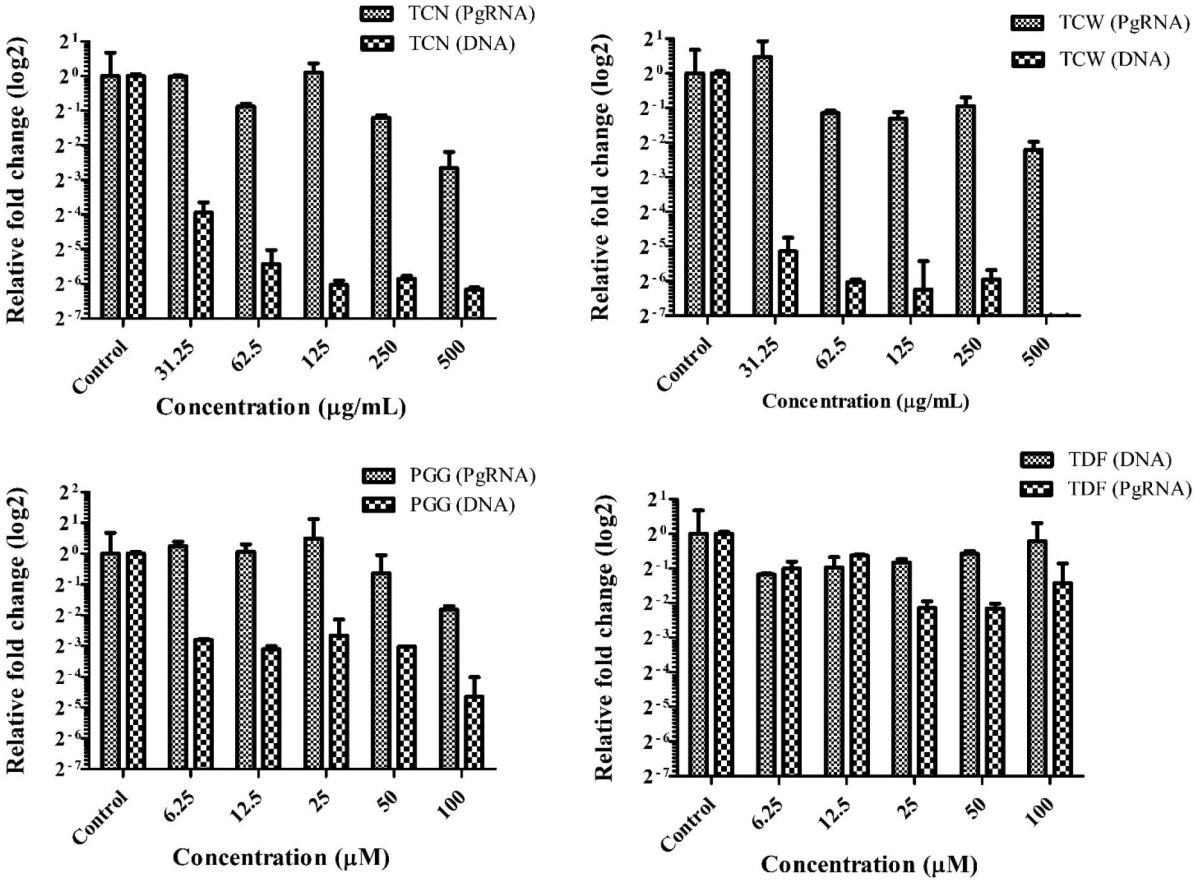

Figure 8. Effect of TCN, TCW, PGG, and TDF treatment on intracellular HBV DNA and pgRNA. HepG2.2.15 cells were treated with or without drugs at the indicated concentrations for 24h. Total intracellular HBV pgRNA and DNA were quantified using qRT-PCR. The results are expressed as the mean ± SEM of two independent biological replicates and two dependent technical replicates.

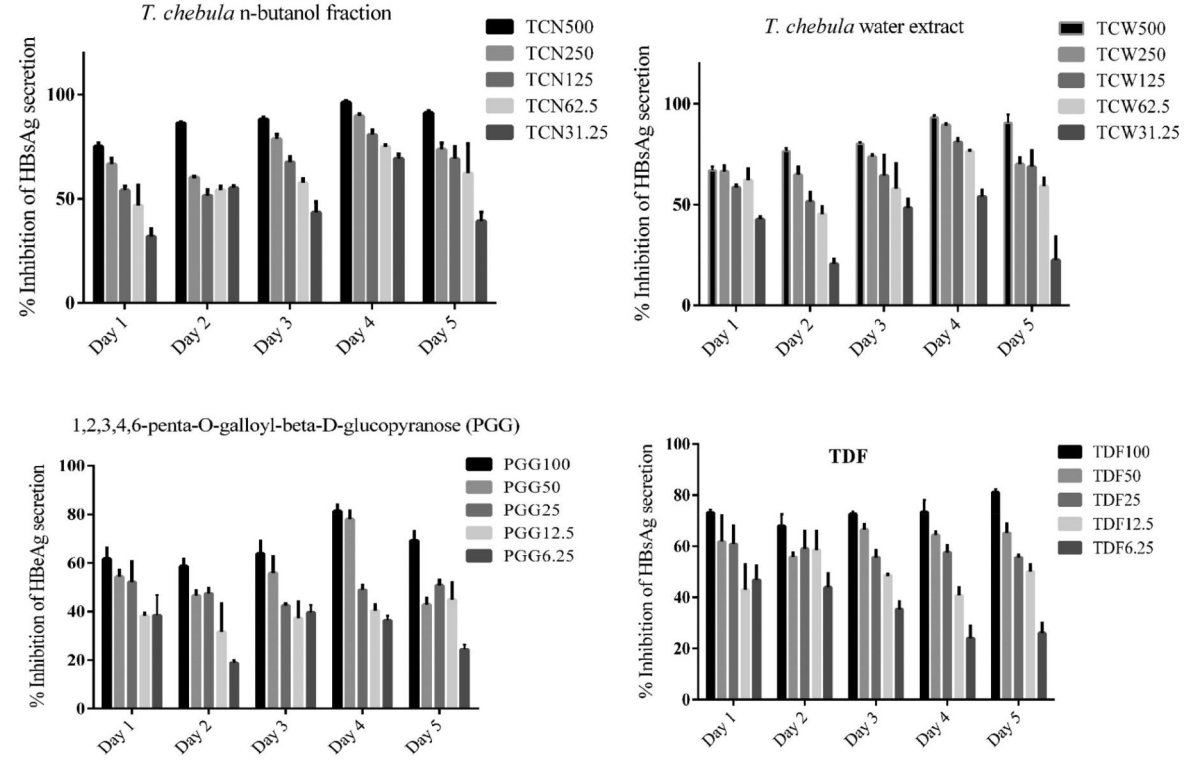

Figure 9. Effect of TCN, TCW, PGG, and TDF on HBsAg level in HepG2.2.15 cell line. The results are expressed as the mean ± SEM of two independent biological replicates.

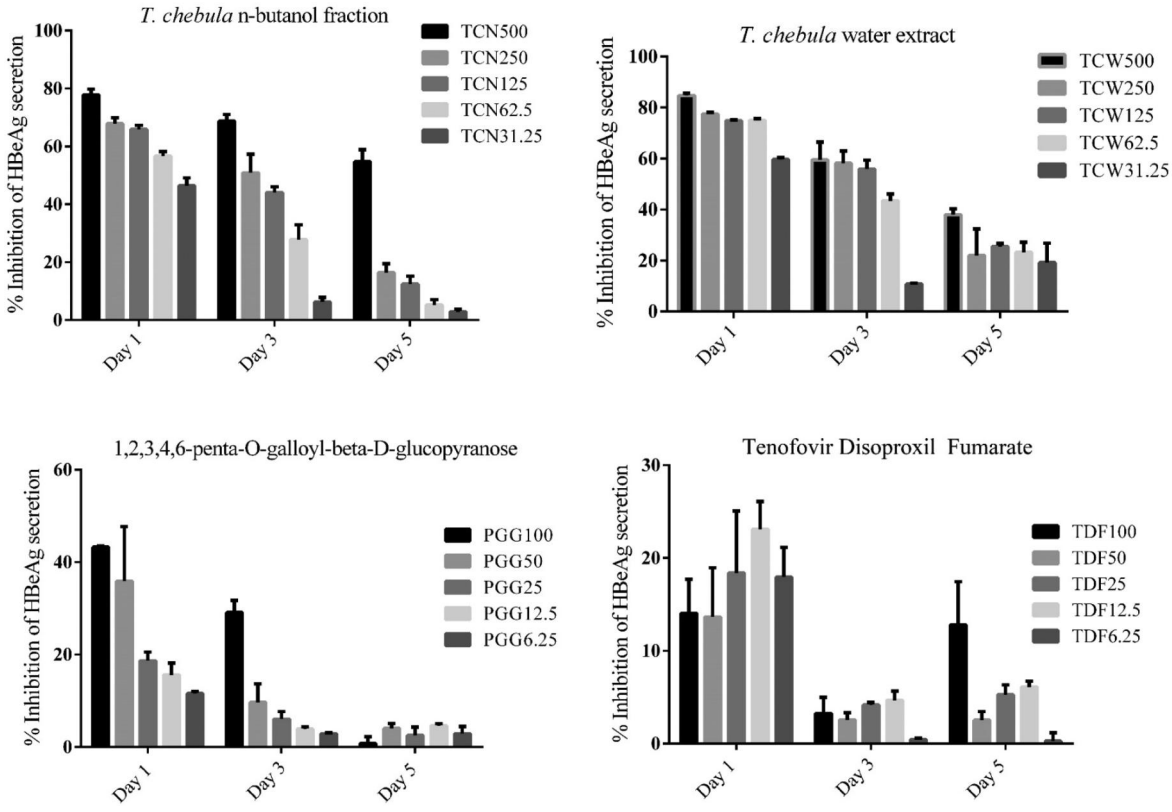

Figure 10. Effect of TCN, TCW, PGG, and TDF on HBeAg level in HepG2.2.15 cell line. The results are expressed as the mean ± SEM of two independent biological replicates and two dependent technical replicates.

methanol (BPM), hydroalcoholic (BPHA) extract, *C. asiatica* hydroalcoholic (CAHA), PGG (pure compound from *T. chebula*), and a standard drug TDF were further evaluated by *in vitro* methods. Initially, LC-MS profiles of *T. chebula*, *B. pilosa*, and *C. asiatica* samples were performed to identify the *in silico* prioritized compounds within the extracts. Each test drug was tested for cytotoxicity in HBV expressing HepG2.2.15 cells. Then, RT inhibitory activity of each test drug was tested using a colorimetric RT inhibitory assay kit, and based on this we prioritized TCN, TCW, PGG, and TDF for further assays. Further, TCN, TCW, PGG, and TDF effects on intracellular HBV DNA and pgRNA in HepG2.2.15 cells were studied. Finally, time and concentration-dependent HBsAg (24, 48, 72, 96, and 120h) and HBeAg (24, 72, and 120h) secretion were studied in HepG2.2.15 cells.

Since the emergence of hepatitis B viral infection, several reports have been published highlighting the construction of the full-length DNA polymerase or its functional domains crystal structures, however existing structures failed to provide complete structural features of its three-dimensional structure (Buhlig et al., 2020; Xu et al., 2016). Therefore, in the present study, we modelled and validated HBV-RT in complex with cofactor Mg^{2+} and known HIV-RT inhibitor. The HBV-RT domain is known as a catalytic center of polymerase, and it has a high degree of homology with HIV1-RT enzyme and both possess conserved multiple catalytic activities (Xu et al., 2016). In this study, Phyre2 server was used to build HBV-RT model, as it comprehensively builds 3D models, predicts ligand binding sites, and analyses the impact of amino acid variants for the given protein sequence using sophisticated 2remote homology detection methods (Kelley et al., 2015). The server mainly utilizes the following components for modeling (a) HHpred v1.51 for template detection, (b) Psi-pred v2.5 for secondary structure prediction, (c) Disopred v2.4 for disorder prediction, (d) Memsat_SVM for transmembrane prediction, (e) Poing v1.0 for multi-template modelling and ab initio (Kelley et al., 2015). LocPREDMD server was used to energy minimize the modelled protein, as it uses molecular dynamics (MD) simulations *via* employing force field-based minimization, refines the structure, and calculates (a) clash score, rotamer outliers (%), Ramachandran outliers from MolProbity, (b) VERIFY3D, (c) G-factor, mainchain bonds (%), mainchain angles (%), sidechain planarity (%) from PROCHECK w.r.t. initial structure (Feig, 2016). The structure obtained from LocPREDMD was submitted to GalaxyREFINE, as it first rebuilds side chains and performs side-chain repacking, followed by overall structure relaxation *via* MD simulation (Heo et al., 2013). Further, in order to retrieve the least potential energy (PE) conformation, all-atom explicit MD simulation was performed by desmond and extracted the lowest PE conformation (-150060.689 kcal/mol). To enhance the structural similarity and accuracy of the modelled protein with respect to a template structure, the active site "YMDD motif" amino acid residue "M204 and D206" position having RMSD >1 was constrained in ModLoop for loop refinement and as a result, the YMDD motif RMSD was found to be <1. On post-refined, about 98.7% of the residues including YMDD were found to span within the favoured region. Further, Modeller with

implementing copy_ligand.py was utilized to build the HBV-RT in complex catalytic Mg^{2+} and known inhibitor at its active site.

Medicinal plants consist of multiple bioactive molecules and deal with polygenic pathogenesis and may pose inhibitory activity against viral protein targets (Pan et al., 2013; Remali & Aizat, 2020). Based on the traditional claims and their efficacy in treating hepatitis-like illness, 18 medicinal plants were shortlisted for this study. In the current approach, the phytocompounds present in these plants were virtually screened against the modelled HBV-RT. As a result, out of 268 phytocompounds, 15 were identified to target YMDD motif and RT1 motif of HBV-RT. The docking study provided more insights on the intermolecular interactions of known inhibitor and phytocompounds with HBV-RT. Among the selected phytocompounds, 6 compounds from *T. chebula*, 5 compounds from *B. pilosa*, and 4 from *C. asiatica* were identified to interact with residues of RT1 motif (aa21-aa51) and YMDD motif residues (aa203-aa206). The RT1 motif consists of G box (aa-24-aa36) and F box (aa37-aa47) (Clark & Hu, 2015), are essential for Hε binding *via* interacting with T3 motif in TP to facilitate packaging of specific pgRNA into viral nucleocapsids and initiation of reverse transcription (Clark & Hu, 2015; Jones & Hu, 2013). Further, in the RNA-dependent DNA polymerase, YMDD motif is highly conserved, as it is involved in nucleotide binding to catalytic site of the polymerase in both HIV and HBV (Bartholomeusz et al., 2004; Ono-Nita et al., 1999). Among the 15 molecules, Terflavin-C and 1,3,6-Tri-O-galloyl-β-D-glucose from *T. chebula* scored the lowest BE of −9.4 kcal/mol and −9.3 kcal/mol, respectively. The structural stability of 15 phytocompounds with HBV-RT was validated by molecular dynamics for 100 ns of production run. All 15 the complexes were found to feature stable backbone and complex RMSD with least residual fluctuation (RMSF) at the ligand-binding site, and showed stable interactions with RT1 and YMDD motif residues throughout 100 ns of production run. To reaffirm the binding affinity, the binding free energy of complexes were also calculated using Prime MMGBSA module. Among the selected compounds, 1,2,3,4,6-penta-O-galloyl-e-D-glucose scored the least binding free energy of −113.774 kcal/mol and the known inhibitor scored −11.069 kcal/mol. Interestingly, other molecules also scored the binding free energy in the range of −87.165 kcal/mol to −26.640 kcal/mol. This information provided phytocompounds as better hit molecules against HBV-RT compared to known inhibitor.

In order to validate these findings, RT inhibitory activity of TCN, TCW, BPM, PBHA, CAHA, PGG, and TDF were performed. TCN (IC_{50} = 147.077 μg/mL), TCW (IC_{50} = 149.214 μg/mL), and PGG (IC_{50} = 149.075 μM) showed potent RT enzyme inhibitory activity in a dose-dependent manner. Whereas, BPM, BPHA, and CAHA didn't show RT inhibitory activity. TDF, a standard molecule didn't show RT inhibitory activity at 250 μM concentration. This is because, TDF is a prodrug and it converts to tenofovir monophosphate (nucleoside/tide) analog and subsequently converts to the active metabolite, tenofovir diphosphate by intracellular AMP kinase. Tenofovir diphosphate inhibits reverse transcriptase/polymerase by direct binding competition with the deoxyadenosine 5′-triphosphate and causes viral DNA chain termination (Kearney et al., 2004). Similarly, we examined the effect of TCN, TCW, PGG, and TDF on intracellular HBV DNA and pgRNA in HepG2.2.15 cell line. Here, TCN and TCW 125, 250, and 500 μg/mL for 24h decreased the intracellular HBV DNA by 2^6 and 2^7 fold and PGG 100 μM also showed about 2^5 fold decrease in intracellular DNA. This indicates all the tested drugs and TDF were effectively impeded the synthesis of viral rcDNA from pgRNA *via* inhibiting the RT enzyme and subsequently inhibiting the formation and secretion of HBV virion. Further, only TCN and TCW 500 μg/mL and PGG100μM showed about 2^2 fold decrease in pgRNA level. This is because, unlike in natural HBV infection, the HepG2.2.15 cells already have the stably integrated HBV genome in HepG2 chromosome. Which is constitutively expressing HBV pgRNA. Hence, these tested drugs and TDF, didn't show a significant effect on pgRNA level.

Further, the effect of TCN, TCW, PGG, and TDF on secretory HBsAg and HBeAg levels in HepG2.2.15 cells were measured at different hours. TCN and TCW exhibited strong HBsAg and HBeAg secretion inhibitory activity (∼80%) compared to PGG and TDF. As time progresses, the inhibition of HBeAg expression/secretion decreased may be due to the time-dependent reduced effect of test drugs on 3.5 kb RNA expression. However, uniform inhibition was observed for all the test drugs throughout the experiment (24 to 120 hrs), due to a strong inhibitory effect on 2.4/2.1 kb RNA expression. The overall *in vitro* findings suggests the TCN, TCW, and PGG were found to be effective against HBV infection by strongly inhibiting RT enzyme and also reducing the synthesis HBsAg and some extent HBeAg and prevent the formation of active HBV particles, which is also evident by decreased intracellular viral DNA levels.

Further, the study is extended to check interactions of phytocompounds with host protein targets and pathways by integrating through gene set enrichment and network pharmacology. This analysis aids in understanding the additional role of these phytocompounds on host targets which are relevant to hepatomodulatory effects (Patil, Harish, et al., 2022). Hence, the host targets of the 15 shortlisted phytocompounds were predicted by BindingDB database. Out of 15 compounds, 11 compounds were predicted to target 75 host proteins. The KEGG enrichment analysis inferred 40.54% of overall pathways involved in HBV infection and its associated complications. The phytocompound-protein-pathway network reflected Okanin, 1,2,3,4,6-penta-O-galloyl-e-D-glucose, and 1,3,6-Tri-O-galloyl-β-D-glucose as the major regulators of the highest count of modulated proteins. Pathways relevant to cancer (KEGG id: hsa05200) were predicted as major components within the network; may possess hepatoprotective beneficial effects over cirrhosis and HCC.

Drug-likeness characteristics are a qualitative concept in computer-aided drug design, assessing based on the knowledge of the structure and properties of atoms for a small molecule for their absorption, biodistribution, bioavailability, and excretion properties. This prediction is generally made in prior to the compounds are isolated from the medicinal plants or synthesized in the laboratory in order to streamline

the wet-lab experiments (Veber et al., 2002). The druggability of phytocompounds were also predicted, which inferred that these 15 compounds to show positive DLS. 1,3,6-Tri-O-galloyl-β-D-glucose scored the highest DLS of 0.92 and Okanin scored the least DLS of 0.23. Further, the biological spectra of 15 phytocompounds were predicted using the PASS server (Pa $\geq$0.3). In this prediction, two of the compounds were not scored as these had a Molcharge of 1. All the other compounds were predicted to possess biological activity as hepatoprotectant (Pa = 0.608 to 0.972), hepatic disorders treatment (Pa= 0.422 to 0.759), and antiviral (Pa = 0.33 to 0.403) properties. Interestingly, out of 13 compounds, 10 compounds showed Pa for hepatitis B (Pa = 0.348 to 0.513) viz., Centaurein (0.479), Okanin-4′-O-glucoside (Marein) (0.402), Okanin 4-methyl ether 3′-glucoside (0.356), Jacein (0.479), Isorhamnetin 3-O-rutinoside (0.428), Castillicetin (0.479), Chebulagic acid (0.348), Tellimagrandin I (0.377), 1,3,6-Tri-O-galloyl-β-D-glucose (0.354), and Terflavin-C (0.513).

T. chebula, B. pilosa, and C. asiatica have been utilized widely in herbal formulation and a long been regarded as Ethnomedicine/folk medicine due to their various therapeutic properties (https://nitmmedplantsdb.in/). *T. chebula* plant is also known as the "King of Medicine" in Tibetan medicine. It is known as "Arura" which means it cures all diseases caused by Vayu, Pitta, Kapha, and clears the diseases of all 7 dhatus (blood, plasma, fat, muscle, nerve/bone marrow, and reproductive tissue) and it is considered to be a great panace and it is listed top of the list of "Ayurvedic Materia Medica" (Bag et al., 2013; Chattopadhyay & Bhattacharyya, 2007; Patil, Harish, et al., 2022; Ratha & Joshi, 2013). *T. chebula* has been shown to have exerted restorative efficacies against malignancy (Li et al., 2018; Shankara et al., 2016), liver toxicity/infection (Choi et al., 2015; Tasduq et al., 2006), diabetes (Murali et al., 2007), inflammation (Yang et al., 2014), etc. Water extract of *T. chebula* is reported to possess anti-apoptotic and anti-necroptotic activity *by* inhibiting tumor necrosis factor-induced necroptosis through the suppression of TNF-induced ROS (Lee et al., 2016). In this current presented study, *T. chebula* constituents were predicted to target apoptosis by targeting the host targets: TNF, TNFRSF1A, TUBA1A, and TUBA1B. Earlier studies have reported that pentagallyol glucose (key compound of *T. chebula*) to downregulate NF-κB, ROS, MMP2, MMP9, TNF, interleukin (IL)-4, 6, 8 etc, and up regulate radical scavenging, SOD, CAT, GSH, LOX, etc (Patnaik et al., 2019). In this study, *T. chebula* constituents were predicted to modulate apoptosis, NF-κB, HIF-1, and mTOR signaling pathway and found to counteract viral protein interactions with cytokine and cytokine receptor. This effect could be due to the presence of pentagallyol glucose moieties. Similarly, *B. pilosa* and *C. asiatica* constituents were also predicted to modulate these pathways and found to play important role in the regulation of HBV infection and associated complications. *C. asiatica* is well reported for its antioxidant and anti-inflammatory activity (Sun et al., 2020). Park et al. (Park et al., 2017) reported the inhibition of NF-κB activation by *C. asiatica* titrated extract. The juice of *C. asiatica* was shown to potentially inhibit the proliferation of malignant HepG2 cell line, thereby can constrain the promotion and tumour invasion (Hussin et al., 2014). *C. asiatica* is also reported to decrease the inflammatory mediator's viz., granulocyte/macrophage colony-stimulating factor, IL-1β, IL-2, 6, 10 and 12, TNF-α, and IFN-γ (Naidoo et al., 2017). *B. pilosa* is rich in chalcones (okanin and its derivatives) (ref), and chalcones are reported to possess broad spectrum antiviral activity against HBV, HCV, herpes simplex, rhinovirus, HIV, cytomegalo, influenza, dengue, etc (Elkhalifa et al., 2021; Nakama et al., 2012) and immunomodulatory (Abajo et al., 2004), anti-inflammatory (Fotso et al., 2014), and protective effect against liver fibrosis (Yuan et al., 2008). Centaurein isolated from *B. pilosa* was reported to regulate IFN-γ transcription *via* nuclear factor of activated T-cells and NF-κB (Chang et al., 2007). In this present study, Centaurein was predicted to modulate 26 protein targets and 15 pathways including NF-κB signaling pathway *via* targeting TNFRSF1A, PLAU, CXCL12, TNF (out of 26 targets).

5. Conclusion

The present study highlights the modelling and validation of HBV-RT structure complexed with Mg^{2+} ion and known inhibitor. Virtual screening and MD simulation studies revealed 15 hit moieties to have greater binding affinity and very stable interaction with the catalytic residues specifically tannins from *Terminalia chebula* (6) and flavonoids from *Bidens pilosa* (5) and *Centella asiatica* (4). These molecules also possess interactions with the host targets involved in the HBV infection and associated complications like HCC. Further, the study identified TCN, TCW, and PGG to potentially inhibit RT, decreased the intracellar DNA and pgRNA, and time-dependent decrease in HBsAg and HBeAg levels in HepG2.2.15 cell line. TCN, TCW, and PGG could be valuable resources for the prevention of HBV infection. The current study is solely based on computational and *in vitro* experimental findings which further animal experiments and clinical validations could be complemented to confirm their therapeutic potential.

Acknowledgments

The authors gratefully acknowledge the extramural funding of the Indian Council of Medical Research, Department of Health Research, New Delhi (ICMR grant No. ISRM/12(61)2019) and the intramural funding of the ICMR-National Institute of Traditional Medicine, Belagavi for providing resources. We also acknowledge the ICMR grant No. ISRM/12(25)/2019 for Schrodinger Prime accessibility. Vishal S. Patil is thankful to the KLE Academy of Higher Education and Research, Belagavi, India, for supporting his Ph.D. studies.

Availability of data and material

All data generated or analysed during this study are included in this published article (and its supplementary information files).

Disclosure statement

The authors declare that they have no known competing financial interests or personal relationships that could have appeared to influence the work reported in this paper.

Funding

This study was funded by the Indian Council of Medical Research, Department of Health Research, New Delhi (ICMR grant No. ISRM/12(61)2019) and ICMR-National Institute of Traditional Medicine, Belagavi, India.

ORCID

Sunil S. Jalalpure http://orcid.org/0000-0001-7598-5973

Authors' contribution

VSP: Main worker, designed and performed the study, writing, and drafting of the manuscript. DRH: Supervised the study, conceptualization, provided inputs, critically reviewed drafts, and finalized the manuscript. RC: Assisted VSP in wet lab experiments. UV: co-supervised VSP on homology modelling, molecular docking, MD simulation, provided inputs, and critically revised the manuscript. VVB, SHD: helped VSP in data mining, analysis, and manuscript writing. SR, SSJ, HH: co-supervised, provided inputs and critical revision of the manuscript. All the authors read and approved the final.

References

Abajo, C., Boffill, M. Á., del Campo, J., Méndez, M. A., González, Y., Mitjans, Mand., & Vinardell, M. P. (2004). In vitro study of the antioxidant and immunomodulatory activity of aqueous infusion of *Bidens pilosa*. *Journal of Ethnopharmacology*, *93*(2–3), 319–323. https://doi.org/10.1016/j.jep.2004.03.050

Adhikari, A., Darbar, S., Das, M., Mondal, S., Bhattacharya, S. S., Pal, D., & Pal, S. K. (2020). Rationalization of a traditional liver medicine using systems biology approach and its evaluation in preclinical trial. *Computational Biology and Chemistry*, *84*, 107196. https://doi.org/10.1016/j.compbiolchem.2019.107196

Bag, A., Bhattacharyya, S. K., & Chattopadhyay, R. R. (2013). The development of *Terminalia chebula* Retz. (Combretaceae) in clinical research. *Asian Pacific Journal of Tropical Biomedicine*, *3*(3), 244–252. https://doi.org/10.1016/S2221-1691(13)60059-3

Bartholomeusz, A., Tehan, B. G., & Chalmers, D. K. (2004). Comparisons of the HBV and HIV polymerase, and antiviral resistance mutations. *Antiviral Therapy*, *9*(2), 149–160. https://doi.org/10.1177/135965350400900203

Bowers, K. J., Chow, E., Xu, H., Dror, R. O., Eastwood, M. P., Gregersen, B. A., Klepeis, J. L., Kolossvary, I., Moraes, M. A., Sacerdoti, F. D., & Salmon, J. K. (2006). *Scalable algorithms for molecular dynamics simulations on commodity clusters* [Paper presentation]. Proceedings of the 2006 ACM/IEEE Conference on Supercomputing (pp. 84-es). https://doi.org/10.1145/1188455.1188544

Buhlig, T. S., Bowersox, A. F., Braun, D. L., Owsley, D. N., James, K. D., Aranda, A. J., Kendrick, C. D., Skalka, N. A., & Clark, D. N. (2020). Molecular, evolutionary, and structural analysis of the terminal protein domain of hepatitis b virus polymerase, a potential drug target. *Viruses*, *12*(5), 570. https://doi.org/10.3390/v12050570

Chang, S. L., Chiang, Y. M., Chang, C. L. T., Yeh, H. H., Shyur, L. F., Kuo, Y. H., Wu, T. K., & Yang, W. C. (2007). Flavonoids, centaurein and centaureidin, from *Bidens pilosa*, stimulate IFN-γ expression. *Journal of Ethnopharmacology*, *112*(2), 232–236. https://doi.org/10.1016/j.jep.2007.03.001

Chattopadhyay, R. R., & Bhattacharyya, S. K. (2007). *Terminalia chebula*: An update. *Pharmacognosy Reviews*, *1*(1), 151–156.

Choi, M. K., Kim, H. G., Han, J. M., Lee, J. S., Lee, J. S., Chung, S. H., & Son, C. G. (2015). Hepatoprotective effect of *Terminalia chebula* against t-BHP-induced acute liver injury in C57/BL6 mice. *Evidence-Based Complementary and Alternative Medicine*, *2015*, 1–11. https://doi.org/10.1155/2015/517350

Clark, D. N., & Hu, J. (2015). Unveiling the roles of HBV polymerase for new antiviral strategies. *Future Virology*, *10*(3), 283–295. https://doi.org/10.2217/fvl.14.113

Coffin, C. S., Mulrooney-Cousins, P. M., & Michalak, T. I. (2021). Hepadnaviral lymphotropism and its relevance to HBV persistence and pathogenesis. *Frontiers in Microbial*, *12*, 695384.

Datta, S., Chatterjee, S., Veer, V., & Chakravarty, R. (2012). Molecular biology of the hepatitis B virus for clinicians. *Journal of Clinical and Experimental Hepatology*, *2*(4), 353–365. https://doi.org/10.1016/j.jceh.2012.10.003

DeLano, W. L. (2002). Pymol: An open-source molecular graphics tool. *CCP4 Newsletter on Protein Crystallography*, *40*(1), 82–92.

Dhama, K., Tiwari, R., Chakrabort, S., Saminathan, M., Kumar, A., Karthik, K., Wani, M. Y., A., Singh, S. V., & Rahal, A. (2013). Evidence based antibacterial potentials of medicinal plants and herbs countering bacterial pathogens especially in the era of emerging drug resistance: An integrated update. *International Journal of Pharmacology*, *10*(1), 1–43. https://doi.org/10.3923/ijp.2014.1.43

Elkhalifa, D., Al-Hashimi, I., Al Moustafa, A. E., & Khalil, A. (2021). A comprehensive review on the antiviral activities of chalcones. *Journal of Drug Targeting*, *29*(4), 403–419. https://doi.org/10.1080/1061186X.2020.1853759

Feig, M. (2016). Local protein structure refinement via molecular dynamics simulations with locPREFMD. *Journal of Chemical Information and Modeling*, *56*(7), 1304–1312. https://doi.org/10.1021/acs.jcim.6b00222

Fiser, A., & Sali, A. (2003). ModLoop: Automated modeling of loops in protein structures. *Bioinformatics (Oxford, England)*, *19*(18), 2500–2501. https://doi.org/10.1093/bioinformatics/btg362

Fontana, R. J. (2009). Side effects of long-term oral antiviral therapy for hepatitis B. *Hepatology (Baltimore, Md.)*, *49*(5 Suppl), S185–S195. https://doi.org/10.1002/hep.22885

Fotso, A. F., Longo, F., Djomeni, P. D. D., Kouam, S. F., Spiteller, M., Dongmo, A. B., & Savineau, J. P. (2014). Analgesic and antiinflammatory activities of the ethyl acetate fraction of *Bidens pilosa* (Asteraceae). *Inflammopharmacology*, *22*(2), 105–114. https://doi.org/10.1007/s10787-013-0196-2

Guo, H., Jiang, D., Zhou, T., Cuconati, A., Block, T. M., & Guo, J. T. (2007). Characterization of the intracellular deproteinized relaxed circular DNA of hepatitis B virus: An intermediate of covalently closed circular DNA formation. *Journal of Virology*, *81*(22), 12472–12484. https://doi.org/10.1128/JVI.01123-07

Heo, L., Park, H., & Seok, C. (2013). GalaxyRefine: Protein structure refinement driven by side-chain repacking. *Nucleic Acids Research*, *41*(Web Server issue), W384–W388. https://doi.org/10.1093/nar/gkt458

Hepatitis B Foundation. (2022). *Treatment options for Hepatitis B-Approved drugs for adults*. https://www.hepb.org/treatment-and-management/treatment/approved-drugs-for-adults/

Herrscher, C., Roingeard, P., & Blanchard, E. (2020). Hepatitis B virus entry into cells. p. *Cells*, *9*(6), 1486. https://doi.org/10.3390/cells9061486

Hussin, F., Eshkoor, S. A., Rahmat, A., Othman, F., & Akim, A. (2014). The *Centella asiatica* juice effects on DNA damage, apoptosis and gene expression in hepatocellular carcinoma (HCC). *BMC Complementary and Alternative Medicine*, *14*(1), 32. https://doi.org/10.1186/1472-6882-14-32

Jefferies, M., Rauff, B., Rashid, H., Lam, T., & Rafiq, S. (2018). Update on global epidemiology of viral hepatitis and preventive strategies. *World Journal of Clinical Cases*, *6*(13), 589–599. https://doi.org/10.12998/wjcc.v6.i13.589

John, A., Sivashanmugam, M., Umashankar, V., & Natarajan, S. K. (2017). Virtual screening, molecular dynamics, and binding free energy calculations on human carbonic anhydrase IX catalytic domain for deciphering potential leads. *Journal of Biomolecular Structure & Dynamics*, *35*(10), 2155–2168. https://doi.org/10.1080/07391102.2016.1207565

Jones, S. A., & Hu, J. (2013). Hepatitis B virus reverse transcriptase: Diverse functions as classical and emerging targets for antiviral intervention. *Emerging Microbes & Infections*, *2*(9), e56–11. https://doi.org/10.1038/emi.2013.56

Karimi, A., Majlesi, M., & Rafieian-Kopaei, M. (2015). Herbal versus synthetic drugs; beliefs and facts. *Journal of Nephropharmacology*, *4*(1), 27.

Kearney, B. P., Flaherty, J. F., & Shah, J. (2004). Tenofovir disoproxil fumarate: Clinical pharmacology and pharmacokinetics. *Clinical*

Pharmacokinetics, *43*(9), 595–612. https://doi.org/10.2165/00003088-200443090-00003

Kelley, L. A., Mezulis, S., Yates, C. M., Wass, M. N., & Sternberg, M. J. (2015). The Phyre2 web portal for protein modeling, prediction and analysis. *Nature Protocols*, *10*(6), 845–858. https://doi.org/10.1038/nprot.2015.053

Khanal, P., Patil, V. S., Bhandare, V. V., Patil, P. P., Patil, B. M., Dwivedi, P. S., Bhattacharya, K., Harish, D. R., & Roy, S. (2022). Systems and in vitro pharmacology profiling of diosgenin against breast cancer. *Frontiers in Pharmacology*, *13*, 1052849. https://doi.org/10.3389/fphar.2022.1052849

Lee, Y., Byun, H. S., Seok, J. H., Park, K. A., Won, M., Seo, W., Lee, S.-R., Kang, K., Sohn, K.-C., Lee, I. Y., Kim, H.-G., Son, C. G., Shen, H.-M., & Hur, G. M. (2016). *Terminalia chebula* provides protection against dual modes of necroptotic and apoptotic cell death upon death receptor ligation. *Scientific Reports*, *6*(1), 25094. https://doi.org/10.1038/srep25094

Li, S., Ye, T., Liang, L., Liang, W., Jian, P., Zhou, K., & Zhang, L. (2018). Anti-cancer activity of an ethyl-acetate extract of the fruits of *Terminalia bellerica* (Gaertn.) Roxb. through an apoptotic signaling pathway in vitro. *Journal of Traditional Chinese Medical Sciences*, *5*(4), 370–379. https://doi.org/10.1016/j.jtcms.2018.11.006

Liang, T. J. (2009). Hepatitis B: The virus and disease. *Hepatology (Baltimore, Md.)*, *49*(5 Suppl), S13–S21. https://doi.org/10.1002/hep.22881

Louten, J. (2016). *Hepatitis viruses* (pp. 213–233). Essential Human Virology. https://doi.org/10.1016/b978-0-12-800947-5.00012-0

Murali, Y. K., Anand, P., Tandon, V., Singh, R., Chandra, R., & Murthy, P. S. (2007). Long-term effects of *Terminalia chebula* Retz. on hyperglycemia and associated hyperlipidemia, tissue glycogen content and in vitro release of insulin in streptozotocin induced diabetic rats. *Experimental and Clinical Endocrinology & Diabetes : official Journal, German Society of Endocrinology [and] German Diabetes Association*, *115*(10), 641–646. https://doi.org/10.1055/s-2007-982500

Muralikumar, S., Vetrivel, U., Narayanasamy, A., N., & Das, U. (2017). Probing the intermolecular interactions of PPARγ-LBD with polyunsaturated fatty acids and their anti-inflammatory metabolites to infer most potential binding moieties. *Lipids in Health and Disease*, *16*(1), 17. https://doi.org/10.1186/s12944-016-0404-3

Naidoo, D. B., Chuturgoon, A. A., Phulukdaree, A., Guruprasad, K. P., Satyamoorthy, K., & Sewram, V. (2017). *Centella asiatica* modulates cancer cachexia associated inflammatory cytokines and cell death in leukaemic THP-1 cells and peripheral blood mononuclear cells (PBMC's). *BMC Complementary and Alternative Medicine*, *17*(1), 377. https://doi.org/10.1186/s12906-017-1865-2

Nakama, S., Tamaki, K., Ishikawa, C., Tadano, M., & Mori, N. (2012). Efficacy of *Bidens pilosa* extract against herpes simplex virus infection in vitro and in vivo. *Evidence-Based Complementary and Alternative Medicine: eCAM*, *2012*, 413453–413410. https://doi.org/10.1155/2012/413453

Nelson, N. P., Easterbrook, P. J., & McMahon, B. J. (2016). Epidemiology of hepatitis B virus infection and impact of vaccination on disease. *Clinics in Liver Disease*, *20*(4), 607–628. https://doi.org/10.1016/j.cld.2016.06.006

Ono-Nita, S. K., Kato, N., Shiratori, Y., Masaki, T., Lan, K. H., Carrilho, F. J., & Omata, M. (1999). YMDD motif in hepatitis B virus DNA polymerase influences on replication and lamivudine resistance: A study by in vitro full-length viral DNA transfection. *Hepatology (Baltimore, Md.)*, *29*(3), 939–945. https://doi.org/10.1002/hep.510290340

Pan, S. Y., Zhou, S. F., Gao, S. H., Yu, Z. L., Zhang, S. F., Tang, M. K., Sun, J. N., Ma, D. L., Han, Y. F., Fong, W. F., & Ko, K. M. (2013). New perspectives on how to discover drugs from herbal medicines: CAM's outstanding contribution to modern therapeutics. *Evidence-Based Complementary and Alternative Medicine: eCAM*, *2013*, 627375–627325. https://doi.org/10.1155/2013/627375

Park, J. H., Choi, J. Y., Son, D. J., Park, E. K., Song, M. J., Hellström, M., & Hong, J. T. (2017). Anti-inflammatory effect of titrated extract of *Centella asiatica* in phthalic anhydride-induced allergic dermatitis animal model. *International Journal of Molecular Sciences*, *18*(4), 738. https://doi.org/10.3390/ijms18040738

Patil, V. S., Deshpande, S. H., Harish, D. R., Patil, A. S., Virge, R., Nandy, S., & Roy, S. (2020). Gene set enrichment analysis, network pharmacology and in silico docking approach to understand the molecular mechanism of traditional medicines for the treatment of diabetes mellitus. *Journal of Proteins and Proteomics*, *11*(4), 297–310. https://doi.org/10.1007/s42485-020-00049-4

Patil, V. S., Harish, D. R., Vetrivel, U., Deshpande, S. H., Khanal, P., Hegde, H. V., Roy, S., & Jalalpure, S. S. (2022). Pharmacoinformatics analysis reveals flavonoids and diterpenoids from *Andrographis paniculata* and *Thespesia populnea* to target hepatocellular carcinoma induced by hepatitis B virus. *Applied Sciences*, *12*(21), 10691. https://doi.org/10.3390/app122110691

Patil, V. S., Harish, D. R., Vetrivel, U., Roy, S., Deshpande, S. H., & Hegde, H. V. (2022). Hepatitis c virus NS3/4A inhibition and host immunomodulation by tannins from *Terminalia chebula*: A structural perspective. *Molecules (Basel, Switzerland)*, *27*(3), 1076. https://doi.org/10.3390/molecules27031076

Patil, V. S., Meena, H., & Harish, D. R. (2021). *Erythrina variegata* L. bark: An untapped bioactive source harbouring therapeutic properties for the treatment of Alzheimer's disease. *In Silico Pharmacology*, *9*(1), 51. https://doi.org/10.1007/s40203-021-00110-0

Patil, P. P., Patil, V. S., Khanal, P., Darasaguppe, H. R., Charla, R., Bhatkande, A., Patil, B. M., & Roy, S. (2022). Network pharmacology and *in vitro* testing of *Theobroma cacao* extract's antioxidative activity and its effects on cancer cell survival. *PloS One*, *17*(4), e0259757. https://doi.org/10.1371/journal.pone.0259757

Patnaik, S. S., Simionescu, D. T., Goergen, C. J., Hoyt, K., Sirsi, S., & Finol, E. A. (2019). Pentagalloyl glucose and its functional role in vascular health: Biomechanics and drug-delivery characteristics. *Annals of Biomedical Engineering*, *47*(1), 39–59. https://doi.org/10.1007/s10439-018-02145-5

Ratha, K. K., & Joshi, G. C. (2013). Haritaki (*Chebulic myrobalan*) and its varieties. *Ayu*, *34*(3), 331–334. https://doi.org/10.4103/0974-8520.123139

Remali, J., & Aizat, W. M. (2020). A review on plant bioactive compounds and their modes of action against coronavirus infection. *Frontiers in Pharmacology*, *11*, 589044. https://doi.org/10.3389/fphar.2020.589044

Samdani, A., & Vetrivel, U. (2018). POAP: A GNU parallel based multithreaded pipeline of open babel and AutoDock suite for boosted high throughput virtual screening. *Computational Biology and Chemistry*, *74*, 39–48. https://doi.org/10.1016/j.compbiolchem.2018.02.012

Seeger, C., & Mason, W. S. (2015). Molecular biology of hepatitis B virus infection. *Virology*, *479-480*, 672–686. https://doi.org/10.1016/j.virol.2015.02.031

Shankara, B. R., Ramachandra, Y. L., Rajan, S. S., Ganapathy, P. S., Yarla, N. S., Richard, S. A., & Dhananjaya, B. L. (2016). Evaluating the anticancer potential of ethanolic gall extract of *Terminalia chebula* (Gaertn.) Retz. (combretaceae). *Pharmacognosy Research*, *8*(3), 209–212. https://doi.org/10.4103/0974-8490.182919

Shannon, P., Markiel, A., Ozier, O., Baliga, N. S., Wang, J. T., Ramage, D., Amin, N., Schwikowski, B., & Ideker, T. (2003). Cytoscape: A software environment for integrated models of biomolecular interaction networks. *Genome Research*, *13*(11), 2498–2504. https://doi.org/10.1101/gr.1239303

Stein, L. L., & Loomba, R. (2009). Drug targets in hepatitis B virus infection. *Infectious Disorders Drug Targets*, *9*(2), 105–116. https://doi.org/10.2174/187152609787847677

Stepanchikova, A. V., Lagunin, A. A., Filimonov, D. A., & Poroikov, V. V. (2003). Prediction of biological activity spectra for substances: Evaluation on the diverse sets of drug-like structures. *Current Medicinal Chemistry*, *10*(3), 225–233. https://doi.org/10.2174/0929867033368510

Sun, B., Wu, L., Wu, Y., Zhang, C., Qin, L., Hayashi, M., Kudo, M., Gao, M., & Liu, T. (2020). Therapeutic potential of *Centella asiatica* and its triterpenes: A review. *Frontiers in Pharmacology*, *11*, 568032. https://doi.org/10.3389/fphar.2020.568032

Tasduq, S. A., Singh, K., Satti, N. K., Gupta, D. K., Suri, K. A., & Johri, R. K. (2006). *Terminalia chebula* (fruit) prevents liver toxicity caused by subchronic administration of rifampicin, isoniazid and pyrazinamide in combination. *Human & Experimental Toxicology*, *25*(3), 111–118. https://doi.org/10.1191/0960327106ht601oa

Toyama, M., Sakakibara, N., Takeda, M., Okamoto, M., Watashi, K., Wakita, T., Sugiyama, M., Mizokami, M., Ikeda, M., & Baba, M. (2019). Pyrimidotriazine derivatives as selective inhibitors of HBV capsid assembly. *Virus Research*, *271*, 197677. https://doi.org/10.1016/j.virusres.2019.197677

Tsukuda, S., & Watashi, K. (2020). Hepatitis B virus biology and life cycle. *Antiviral Research*, *182*, 104925. https://doi.org/10.1016/j.antiviral.2020.104925

Tu, T., Patel, K., & Shackel, N. A. (2017). Chapter 17: Viral Hepatitis. *Genomic and Precision Medicine* (3rd Ed., pp. 317–340). Academic Press. https://doi.org/10.1016/B978-0-12-800685-6.00017-5. https://www.sciencedirect.com/science/article/abs/pii/B9780128006856000175

Umashankar, V., Deshpande, S. H., Hegde, H. V., Singh, I., & Chattopadhyay, D. (2021). Phytochemical moieties from Indian traditional medicine for targeting dual hotspots on SARS-CoV-2 spike protein: An integrative in-silico approach. *Frontiers in Medicine*, *8*, 672629. https://doi.org/10.3389/fmed.2021.672629

Veber, D. F., Johnson, S. R., Cheng, H. Y., Smith, B. R., Ward, K. W., & Kopple, K. D. (2002). Molecular properties that influence the oral bioavailability of drug candidates. *Journal of Medicinal Chemistry*, *45*(12), 2615–2623. https://doi.org/10.1021/jm020017n

Vinayak, U., Hegde, H. V., Divakar, M., Shankar, B., Veeresh, H., & Kholkute, S. D. (2010). Digital database on ethno-medicinal plants of Western Ghats. *Current Science*, *99*(12), 1658–1659.

World Health Organization. (2021). *Hepatitis B*. https://www.who.int/news-room/factsheets/detail/hepatitis-b

Xu, X., Thai, H., Kitrinos, K. M., Xia, G., Gaggar, A., Paulson, M., Ganova-Raeva, L., Khudyakov, Y., & Lara, J. (2016). Modeling the functional state of the reverse transcriptase of hepatitis B virus and its application to probing drug-protein interaction. *BMC Bioinformatics*, *17*(8), 583–592.

Yang, M. H., Ali, Z., Khan, I. A., & Khan, S. I. (2014). Anti-inflammatory activity of constituents isolated from *Terminalia chebula*. *Natural Products Communications*, *9*(7), 1934578X1400900. https://doi.org/10.1177/1934578X1400900721

Yuan, L. P., Chen, F. H., Ling, L., Dou, P. F., Bo, H., Zhong, M. M., & Xia, L. J. (2008). Protective effects of total flavonoids of *Bidens pilosa* L.(TFB) on animal liver injury and liver fibrosis. *Journal of Ethnopharmacology*, *116*(3), 539–546. https://doi.org/10.1016/j.jep.2008.01.010

Zhang, Y., Zhao, Y., Lin, X., Wang, A., & Che, D. (2018). Modeling for the prediction of Hepatitis B incidence based on integrated online search indexes. *Informatics in Medicine Unlocked*, *10*, 143–148. https://doi.org/10.1016/j.imu.2018.01.004

Zoulim, F., & Locarnini, S. (2009). Hepatitis B virus resistance to nucleos(-t)ide analogues. *Gastroenterology*, *137*(5), 1593–1608.e2. https://doi.org/10.1053/j.gastro.2009.08.063